


In Situ Experiments: Paving Ways for Rapid Development of Structural Metallic Materials for a Sustainable Future

Vivek Kumar Sahu¹, Reshma Sonkusare^{1,2}, Krishanu Biswas¹ and N. P. Gurao^{1*} 

Abstract | In situ characterization, experiments provide multi-scale hyperdimensional data on the evolution of microstructure, texture and residual stress as a function of external stimuli providing direct evidence of operative mechanisms as they happen. Combined with computational approaches high throughput in situ or in operando experiments provide a robust methodology for mechanistic mechanism-guided materials and process development. The advancement of high throughput experiments using different probes like visible light, electrons, neutrons and x-rays combined with peripheral equipment enable probing of the different classes of materials over a wide range of processing and service conditions with valuable information in real-time. The development of the materials genome initiative and integrated computational materials engineering have reduced the timeframe for materials and process development and in situ characterization forms an integral part of this approach. In the present review, we highlight different in situ characterization techniques that have helped in unravelling fundamental processes in deformation, recrystallization, phase transformation and failure of metallic materials and components in service. A kaleidoscopic view of the journey of the materials science community through the in situ experimentation landscape with a major focus on research in complex concentrated alloys and additive manufacturing will be followed with a roadmap and a wish list for the future.

Keywords: *In situ characterization, High throughput experiments, Metallic materials sustainability*

1 Introduction

Metallic materials have shaped human civilizations by providing copper mirrors for aesthetics to iron ploughs for agriculture and enabling victories of one civilization with a superior sword material over other from the early days to making commercial space tourism a reality today^{1,2}. The application of metallic materials for structural applications is expected to play an important role in the future with stringent operating conditions in the energy sector including oil and gas, nuclear, high-speed transportation and future

human space missions^{3,4}. In addition to the envisioned applications, the depleting resources for metallic materials in terms of leaner ores and the huge impact of mining on the environment pose a challenge for the application of metallic materials in the world^{5,6}. For a developing country like India, it is a bigger challenge to choose between increasing the production of steel to fulfil its infrastructure needs and providing employment to a large young population at the cost of environmental damage that affects the young and old, rich and poor alike^{5,6}. Thus, the production

¹ Department of Materials Science and Engineering, Indian Institute of Technology Kanpur, Kanpur 208016, India.

² Institute of Applied Materials (IAM-WK), Karlsruhe Institute of Technology, 76344 Eggenstein-Leopoldshafen, Germany.
*npgurao@iitk.ac.in

and application of metallic materials in different industries pose a double-edged challenge which needs urgent attention as things cannot go as usual. An increase in strength of a structural metallic material without compromise in ductility and toughness with a reasonable cost can reduce the size of the component, reducing the volume of material produced thus reducing environmental damage. Similarly, the use of scrap in metal manufacturing can take care of the huge waste littering mother earth while superior mechanical properties across temperature regimes can help in operating a crude oil extraction facility in the arctic or run coal-based power plants at higher temperatures to obtain clean energy. The current pandemic has only amplified the need to take a break and rethink our strategy to re-establish our relationship with nature. Even before the pandemic, extensive work on reimagining the industrial framework in terms of Industry 4.0 and the internet of things was pursued by the academic community and it is expected to rapidly develop in the post-pandemic world⁷⁻¹⁰. This essentially necessitates decentralizing or democratizing the materials manufacturing industry. Coincidentally, two of the major developments in materials and process development in material science and engineering follow the same principle. The development of complex concentrated alloys also known as high entropy alloys are defined as multi-principal multicomponent alloys that can offer excellent mechanical properties comparable or superior to that of conventional alloys has generated a lot of interest of researchers in the metallurgical field⁷⁻¹⁰. Similarly, additive manufacturing processes have the potential to shut down big factories that provide jobs and cheap products to millions but affect the environment and human health in the long term¹¹⁻¹³. Thus, saddled between the twin realities of materialistic development for the betterment of the population and the severe impact on health and the environment, policymakers have to do a tightrope walk.

Scientists and engineers are expected to provide an insight on this matter to the decision-makers based on a thorough scientific background in a short span of time. It is, therefore, important for the community to find a balance between curiosity-driven research and research with societal implications. It is indeed clear that one cannot continue with the status quo and there is a need to reimagine research in these challenging times. Efforts have already been directed in this direction with the evolution of materials genome initiative and integrated computational

materials engineering to take advantage of the huge progress made in terms of computational capacity available with us¹⁴⁻¹⁷. Materials and process simulations across the length and time scales and multi-scale simulations have helped in the design and development of new materials and processes in the last twenty-odd years¹⁸⁻²⁰. Development of the materials genome initiative and integrated computational materials engineering (MGI-ICME) has provided a major boost to new materials and processes. It is expected to help the development of metallurgical processes²¹⁻²⁵ and materials from lab-scale technological readiness level (TRL) to component scale TRL in a short span of time. With the advent of machine learning (ML) and artificial intelligence (AI), the development of new materials and processes has reached greater heights which cut across disciplines and the successful development of vaccines in a record time shows the unique ability of these methods²⁶⁻³⁰. Experiments including sophisticated characterization tools like atom probe tomography correlative microscopy; controlled process conditions like single and bicrystal growth, micro-gravity or levitation solidification and high throughput experiments like combinatorial deformation and microscopy form an integral part of the MGI-ICME paradigm. High throughput experimentation involves a battery of techniques to carry out synthesis, testing, characterization and combinatorial studies across different length and time scales to screen a lot of compositions and process parameters in a short time to facilitate rapid development of new materials and processes. In situ or in operando experiments form a subset of high throughput experiments which offer simultaneous materials characterization when a material is subjected to an external mechanical, thermal, electric, magnetic field or a combination of different fields in the different environments³¹⁻³⁶.

Materials characterization has been central to establishing the structure-processing-property linkages in a broad range of materials including structural materials by providing complete information of the microstructure as a function of different processing steps and service performance. This information has been used to optimize processing steps, improve service performance, understand damage evolution and avoid catastrophic failure. However, the conventional role of materials characterization has been chronological wherein characterization techniques offered insights about the operative mechanisms associated with materials after the process or testing was performed. This sequential nature of

analysis is slow and fraught with errors. There is always a desire to observe operative mechanisms as they happen to establish a mechanistic structure–property–performance paradigm for the development of materials and processes. With this desire, in situ or in operando techniques were developed and though costly compared to traditional process or test and then characterize paradigm, in operando techniques offer a high throughput method that provides a better fundamental understanding of materials and processes that can play an important role in the twenty-first century^{21,37,38}.

Accelerated materials and process development through high throughput experiments that combine testing and characterization for instance nanoindentation with scanning electron microscope-based electron backscatter diffraction (SEM-EBSD), in situ microscopy using optical, scanning and transmission electron microscopy, in situ electron backscatter diffraction, in situ x-ray, neutron and synchrotron diffraction as well as tomography have been established over the years. These techniques cover a wide range of materials including different structural materials, functional materials, catalysts, drugs as well as different processes like fuel cell operation and additive manufacturing processes for metals and ceramics. Micromechanical experiments like pillar compression, beam bending and in situ experiments are useful for mechanical property characterization at a small length scale to study size effect and address fundamental scientific issues. On the other hand, in situ characterization-based experiments like in operando SEM, EBSD, neutron and synchrotron diffraction can aid in the understanding of micro-mechanisms of plastic deformation and damage. The latter needs to be coupled with conventional bulk scale experiments to obtain representative mechanical properties of the bulk. Thus, in situ characterization is important for the process as well as materials development. Metallic materials from solidification to deformation, recrystallization and phase transformation as well as damage accumulation due to deformation or environment leading to final failure can be captured by in situ experiments and correlated with different mechanisms. Such an approach is a mechanism-based approach for materials or process development rather than a trial-and-error method. With AI-ML and the present understanding of thermodynamics and kinetics of different processes, deep learning methodology can be applied for data obtained from high throughput characterization experiments coupled with a few conventional

experiments for targeted development of materials and processes of the next century. This forms the basis of ICME, wherein multiscale simulations are coupled with high throughput experiments that are the bedrock of materials development.

2 Overview of Materials Characterization Techniques

Materials characterization enables the study of the microstructure of materials and forms the basis of the discipline of materials science and engineering, which deals with microstructural design to achieve desired performance from materials. The microstructure of material includes different attributes such as size, shape, morphological and crystallographic orientation of different phases, chemistry and crystal structure, and residual stress as given in Table 1, which can be characterized using different microscopy, diffraction and spectroscopy techniques^{39–46}. It is important to keep the capability and limitations of the different techniques with particular emphasis on resolution, sensitivity and accuracy of different techniques to obtain reliable information about the microstructure at different length scales. Optical microscopy based on focusing visible light to construct images for the samples in transmission or reflection mode is one of the most widely used microstructural characterization tool⁴⁷. The light microscope offers a wide effective characterization scale from centimetre to micrometre with poor depth of field. Electron microscopy⁴⁸ probes the samples with electron beams and offers a wide range of signals for imaging as well as diffraction to provide information about crystal structure and crystal orientation. Scanning and transmission electron microscopy are the two most widely used techniques that offer simultaneous information from the real space and the reciprocal space from the region with sufficient spatial and angular resolution⁴⁹. SEM is characterized by simple sample preparation and excellent depth of field and higher resolution compared to an optical microscope. The development of different imaging signals like secondary electrons, backscattered electrons, specimen current as well as spectroscopy techniques like energy and wavelength dispersive spectroscopy as well as cathodoluminescence and Auger spectroscopy makes the SEM a versatile tool to study the microstructure of the material at different length scales⁵⁰. In addition, the presence of diffraction-based techniques including the most important electron backscatter diffraction technique as

Table 1 Constituents of microstructure of crystalline materials with the avenues to extract microstructural information from the real and reciprocal space³⁵⁻⁴⁶

Description	Information	Measuring technique	Resolution	Examples
Phase fraction, size, shape morphology, composition, interfaces, defects	Real space	Imaging	Spatial resolution	
Crystal structure, orientation	Reciprocal space	Diffraction	Angular resolution	
Micro-strain, residual stress	Reciprocal space	Diffraction	Angular resolution	

well as electron channelling contrast imaging, transmission Kikuchi diffraction and transmission scanning electron microscopy along with relatively easy sample preparation makes SEM the most dominant and versatile characterization technique. Transmission electron microscopy is by far the most sophisticated and powerful materials characterization technique that offers a wide range of imaging, diffraction, defect characterization and spectroscopy tool that is available to a materials scientist⁴⁹. TEM can offer information about microstructure and defect structure from bright and dark field imaging and compositional information from high angle annular dark-field imaging, energy dispersive spectroscopy and electron energy loss spectroscopy; grain orientation information from orientation imaging in a TEM; atomic-level structure from high-resolution TEM and scanning transmission electron microscopy along with basic crystal structure from techniques like converging beam electron diffraction. Thus, the TEM offers a single platform to perform structure determination, chemistry, microstructure and defect characterization to a very high level of precision from a small volume of material.

X-ray characterization techniques utilize electromagnetic x-ray radiation for diffraction, absorption spectroscopy, photoelectron spectroscopy, X-ray microscopy and tomography to provide crucial information from mesoscale morphology to microscale crystal structure and elemental content of different phases in a material^{51–53}. X-rays offer excellent resolution in the diffraction space and are the most versatile for defect characterization at different length scales and provide information on structure, lattice parameter, dislocation density, texture or preferred orientation of crystallites as well as residual stresses. Synchrotron sources offer a wide range of radiations including hard and soft x-rays with very high intensity that can be utilized for localised diffraction, 2D imaging, fluorescence spectroscopy and tomography including diffraction contrast tomography that can provide the complete description of the microstructure in terms of phase morphology, composition by fluorescence, localised atomic structure by x-ray absorption fine structure and residual stress in 3D^{54,55}. The techniques based on neutrons are quite similar to the electron, and neutrons are preferable for analyses of light elements such as lithium. Neutrons have a weak interaction with matter as they interact with the nucleus of the atom and have high penetration depth in solids which helps in obtaining information of microstructure, texture

that is preferred orientation of crystallites and residual stress from the bulk that is at the length scale of an actual engineering component like pipeline steel or a pressure vessel^{56,56}. In addition, neutrons provide information about the material's magnetic properties, which is not accessible by optical, electron or x-rays and are finding more and more applications in functional materials development⁵⁶. All the aforementioned techniques provide a detailed information about the microstructure, structure and chemistry of materials at different length scales and are routinely used for post mortem characterization to decipher the operative micro-mechanisms of phase transformation, deformation, recovery, recrystallization, grain growth as well as damage accumulation by crack formation and growth, void formation, growth, coalescence and ultimate fracture. A brief overview of the capabilities of different characterization tools is presented in Fig. 1a.

3 Need for In Situ Studies

Unlike the conventional application of materials characterization techniques in post-mortem analysis of materials, in situ or in operando techniques combine the aforementioned characterization tools with peripheral equipment or instrumentation that can provide external stimuli like temperature, force or displacement field, magnetic and electric field or multiple fields in a controlled environment or vacuum to the material under observation. It is, therefore, imperative that the peripheral equipment is compatible with the characterization tool and there is minimum interference from the equipment or the external field on the quality of data acquisition. The signal-to-noise ratio for the output in the presence of peripheral equipment is important to obtain a significant signal from the in situ experiment. Peripheral equipment can include a simple hot plate in an optical microscope to a sophisticated environment-controlled furnace with a transparent x-ray window for a laboratory X-ray diffractometer or a beamline on a synchrotron or neutron source. Similarly, mechanical stimuli can be applied by miniature tensile stage or a custom-built tensile, compression, fatigue and three-point bend set up for a SEM of a nano indenter in a TEM. There are a lot of emphasis on developing micro electromechanical system (MEMS) devices to perform in situ experiments in TEM as well as develop dynamic electron microscope to study rapidly occurring processes like dislocation generation, annihilation and interaction with other dislocations and defects. It is also possible

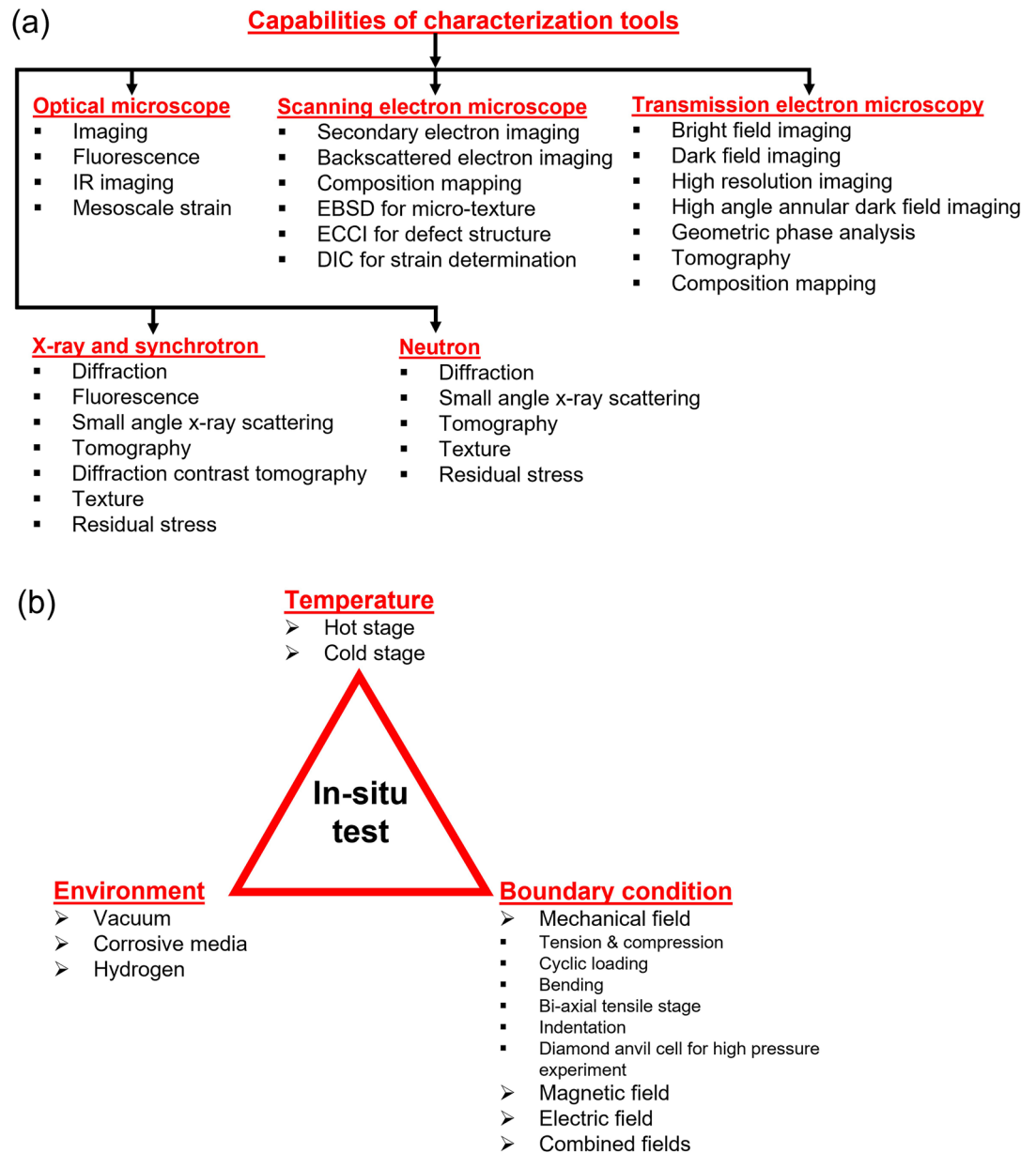


Figure 1: a Capabilities of different characterization techniques. **b** Different variables of in situ test experiments.

to study different modes of loading like tension, compression, shear and bending across different strain rates to study the deformation mechanisms in further detail. Dedicated gas cells and liquid cells are also available for TEM, which enable testing in a controlled atmosphere in the small sample size used in TEM, which is by far the most stringent requirement for peripheral instruments that make in operando studies possible. Similar large-scale mechanical testing equipment in different modes and environment chambers are

available for x-ray, synchrotron and neutron radiation techniques. The major challenge is to ensure that the equipment does not interfere with the diffraction setup or tomography data collection setup. Of late, there has been an increased interest to carry out multi-scale diffraction studies coupled with mechanical testing to study the defect structure at different length scales to develop a fundamental understanding of the operative micro-mechanisms. The philosophy for designing in situ experiments that combine basic materials

characterization with a fixed variable for different environments presented in Fig. 1b.

4 In Situ Experiments Across Real and Reciprocal Space

4.1 Optical Techniques

In situ experiments in an optical microscope employ a reflection microscope with a hot stage for studying melting, solidification, sintering, densification and dimensional changes to study different metallurgical processes. Earlier investigations focused on studying change in contact angle as a function of change in temperature of chemistry as well as wetting and bonding of solid–liquid interface. In situ optical microscopy has been gathering importance in the last decade or so due to the advancement in instrumentation like optical fibre technology and optics that have made it the most important tool in studying various processes in electrochemical energy devices like batteries and cells. The mechanochemical process of lithiation in lithium-ion batteries has been investigated in a detailed manner using in situ optical microscopy to observe the growth of lithium dendrites but also for the evolution of stress in the silicon due to delithiation (Fig. 2a, b)⁵⁷. A major emphasis is to build custom devices to facilitate in situ characterization of electrochemical energy devices to monitor different chemical reactions as they happen and determine the causes of failure due to different processes. Efforts are directed to perform thermal imaging and observe the entire lifetime performance of a battery or a cell including a fuel cell and correlate with failure processes like short-circuiting due to Zn dendrite as shown in Fig. 2c⁵⁷.

4.2 Electron-Based Techniques

4.2.1 Scanning Electron Microscope

In situ electron microscopy techniques employ special holders for applying mechanical, thermal loads as well as the electric and magnetic field in a vacuum or a controlled environment in a scanning electron microscope (SEM) and a transmission electron microscope (TEM). Different modes of mechanical loading like tension, compression, fatigue, bending, indentation over a wide range of strain rates in monotonic and cyclic loading can be applied in SEM and TEM. A SEM offers higher spatial resolution and better depth of field compared to an optical microscope and is better suited to study deformation, recrystallization, phase transformation and damage evolution at the mesoscale. One of the most common peripheral devices is an in situ mechanical testing setup in a SEM (Fig. 3a). This setup can provide deformation of substandard tensile specimen in tension, compression, bending in monotonic and cyclic loading in the quasi-static strain rate regime⁵⁷. Combined with a heating element, such a stage can provide a thermomechanical simulator with limited ability inside a SEM that can provide high-speed, high-resolution secondary electron images of the sample providing detailed information about the evolution of surface morphology, slip lines, crack formation, void nucleation, growth and coalescence. Similarly, recrystallization and phase transformation can also be observed from the SE or BSE imaging (Fig. 4c). In addition to testing in different modes of deformation, there have been efforts to carry out mechanical testing in different corrosive environments using an electrolytic cell in

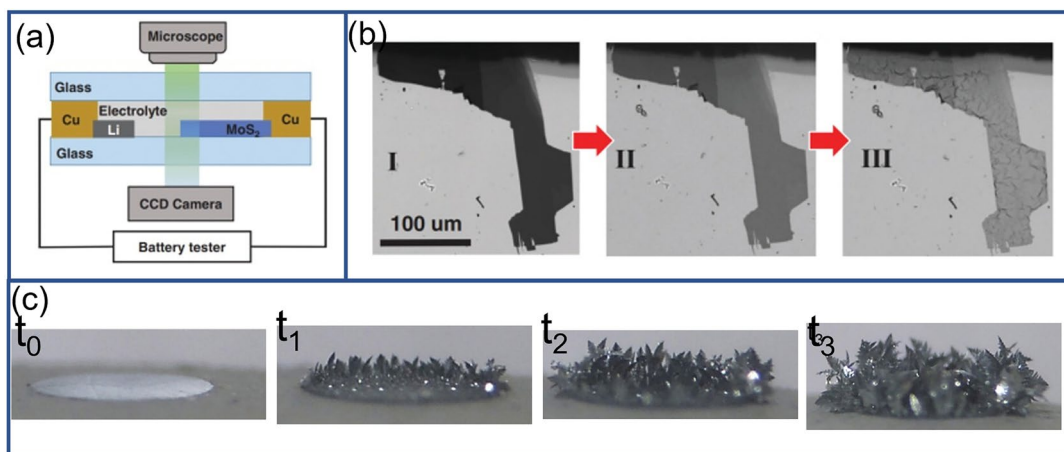


Figure 2: **a** Schematic of the micro battery, **b** a MoS₂ flake at different lithiation stage. **c** The evolution of Zn dendrite at different time⁵⁷.

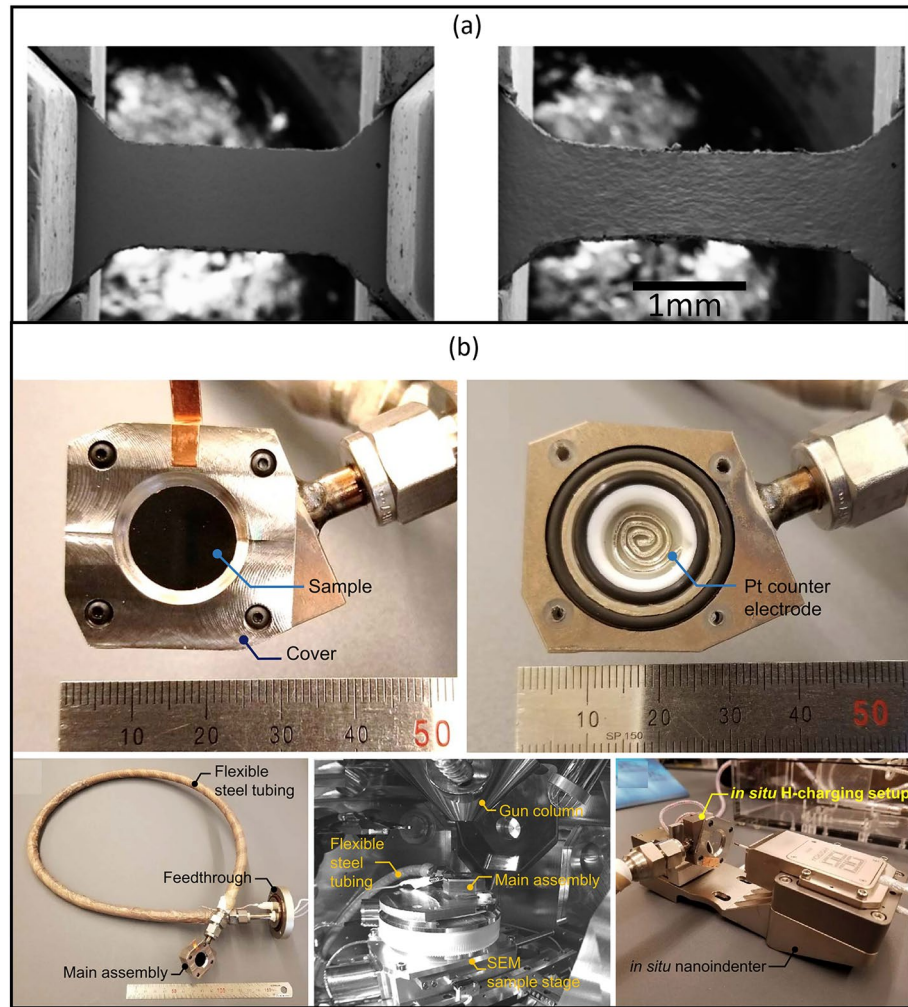


Figure 3: a In situ SEM images and b In situ hydrogen charging setup⁵⁷.

an environmental SEM. Recently there has been an emphasis to study the role of hydrogen on the deformation behaviour of metals and alloys from a scientific as well as technological perspectives. The increasing importance of hydrogen economy for a greener and cleaner future has necessitated the development of metallic materials that can withstand high hydrogen concentrations. The role of hydrogen in the deformation behaviour of metallic materials has gathered interest for the last century and many fundamental issues like developing the understanding of hydrogen enhanced local plasticity, hydrogen enabled decohesion and dislocation and crack interaction with mobile and trapped hydrogen in different metallic materials are not yet addressed⁵⁷. Hence in situ mechanical testing in the presence of gaseous hydrogen or electrochemical hydrogen has been attempted by different groups in the world presently and its setup is shown in Fig. 3b. In situ

mechanical stages used in a SEM are not stiff like a conventional universal tensile machine and hence, stress-strain data obtained from in situ tests is fraught with errors particularly in the measurement of strain. Therefore, digital image correlation (DIC) is employed on SEM images to accurately determine strain in the sample. It is to be mentioned here that the DIC is based on measuring the displacement of random pattern on the sample surface by capturing multiple images of the sample using a high-resolution camera. However, the process of image formation in a SEM is on the basis of scanning rather than projection and hence applying existing DIC algorithms to determine strain is fraught with error. Image shift due to beam drift contributes to ghost strain and necessary care is required to accurately determine strain from DIC applied to SEM images. Nevertheless, the information obtained from in situ tensile or compression or bending test can be

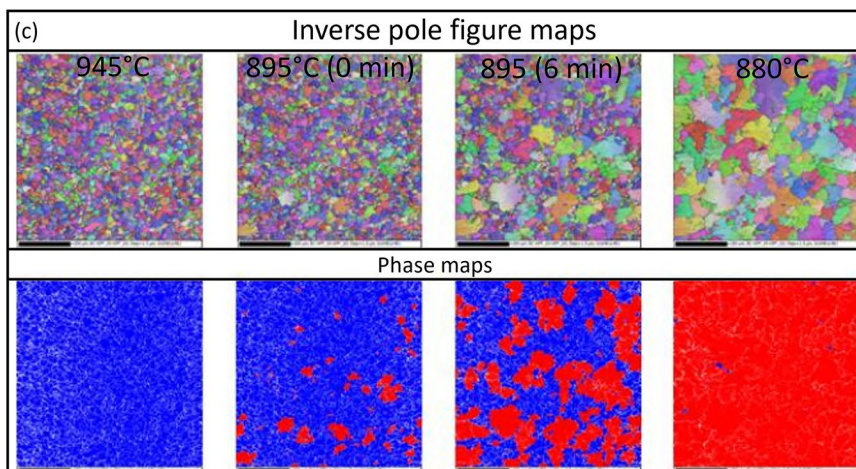
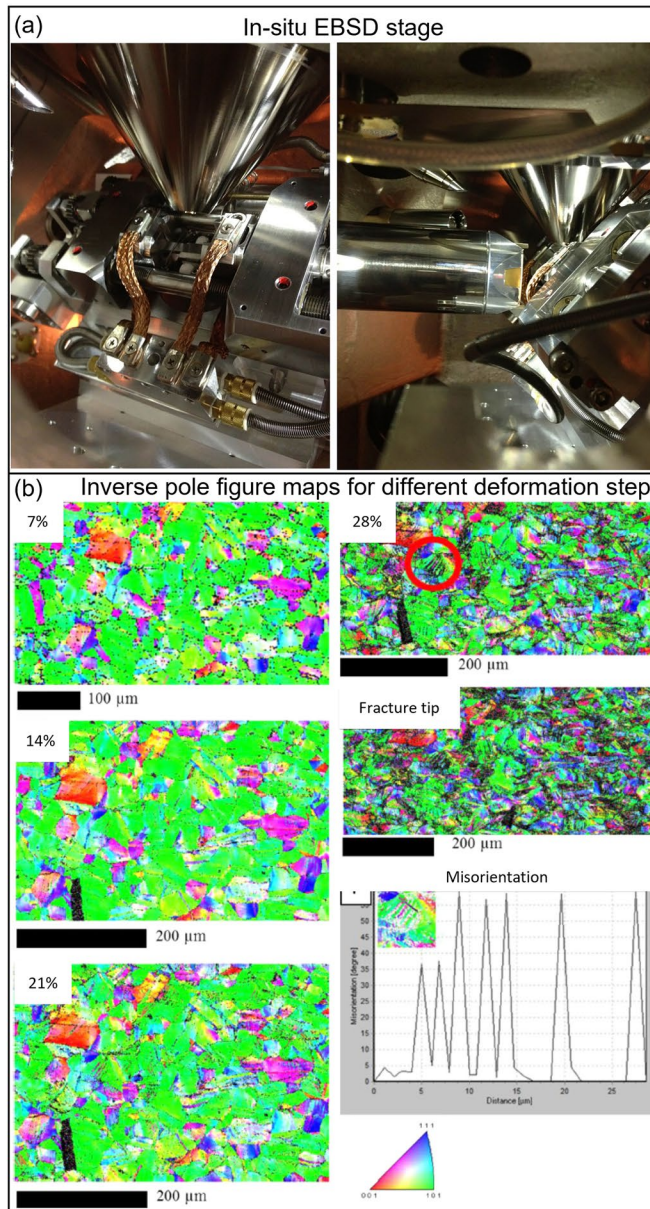


Figure 4: **a** In situ EBSD setup and **b** Inverse pole figure maps along tensile axis at different strain steps in SS 316L⁵⁰. **c** IPF maps for different temperature and time steps during cooling and holding⁵⁰.

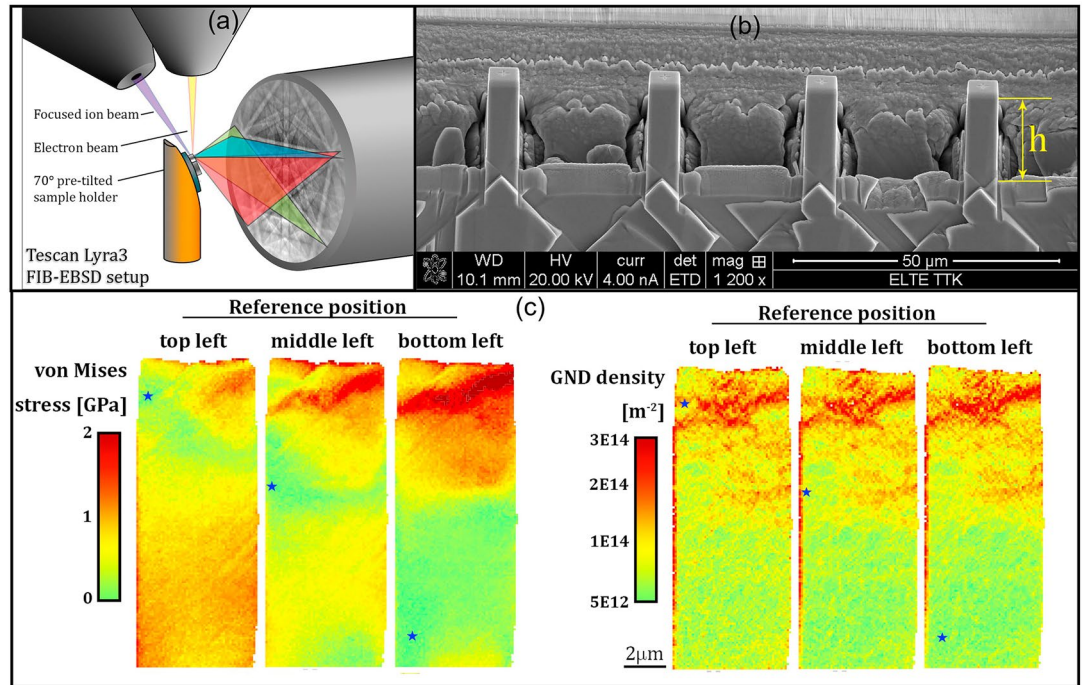


Figure 5: **a** FIB-EBSD setup, **b** micropillar compression with dimension of $6\ \mu\text{m} \times 6\ \mu\text{m} \times 18(h)\ \mu\text{m}$ and **c** von Mises stress and GND density maps at different reference position at 0.7% deformation⁶⁰.

complimented with post deformation EBSD or EDS to determine the orientation of grains and character of grain boundaries as well as composition at the microstructure level to establish a link between the micro-texture, composition and mechanical performance including failure. In situ mechanical testing in a SEM can be modified to allow simultaneous EBSD possible and its setup is shown in Fig. 4a, which makes a very potent device that offers information from the real and reciprocal space as a function of mechanical loading. One example of the evolution of orientation at different deformation steps of SS 316L is given in Fig. 4b which shows extensive deformation twinning in the microstructure with an increase in strain. It was shown that twinning contributes to strain hardening by promoting dynamic Hall-Petch effect caused by reduction in grain size due to twinning till the ultimate tensile strength and then contributes to damage accumulation at twin matrix interface for post-necking deformation. Other valuable information like change in orientation of grains, slip and twinning systems, dislocation density evolution as well as intragranular misorientation can be obtained from postprocessing of the data⁵⁸. Local recrystallization mechanisms as well as phase transformation orientation relationships can also be observed as shown in Fig. 4c. Combined EBSD and EDS can

help us to map the compositional and orientation space of different phases in the microstructure in 2D providing greater insight into micro-mechanisms of deformation, recrystallization and phase transformation⁵⁹. Kalácska et al.⁶⁰ carried out 3D high angular resolution EBSD (3D HR-EBSD) of copper single crystal micropillars prepared by dual-beam scanning electron microscope–focused ion beam (SEM–FIB) with an in situ nanoindentation facility for compression strain of 0.7%, 4% and 10%. (Fig. 5a, b). 3D HR-EBSD on each slice of (001) side prepared by FIB was performed and von Mises stress and geometrically necessary dislocation (GND) density value at three different reference positions of the 0.7% deformed sample (Fig. 5c) showed a good match highlighting the critical role of GNDs in small length scale deformation behaviour of materials.

4.2.2 TEM

In situ experiments in a TEM were probably one of the first in operando experiments performed to study the micro-mechanisms as they happen in materials. Ray et al.⁶¹ studied recrystallization of copper (Fig. 6) in HVTEM to capture the process of recrystallization way back in 1975. Recently, Tiwari et al.⁶² studied the melting behaviour of the nano particles of tri-phasic Bi-In-Sn alloys

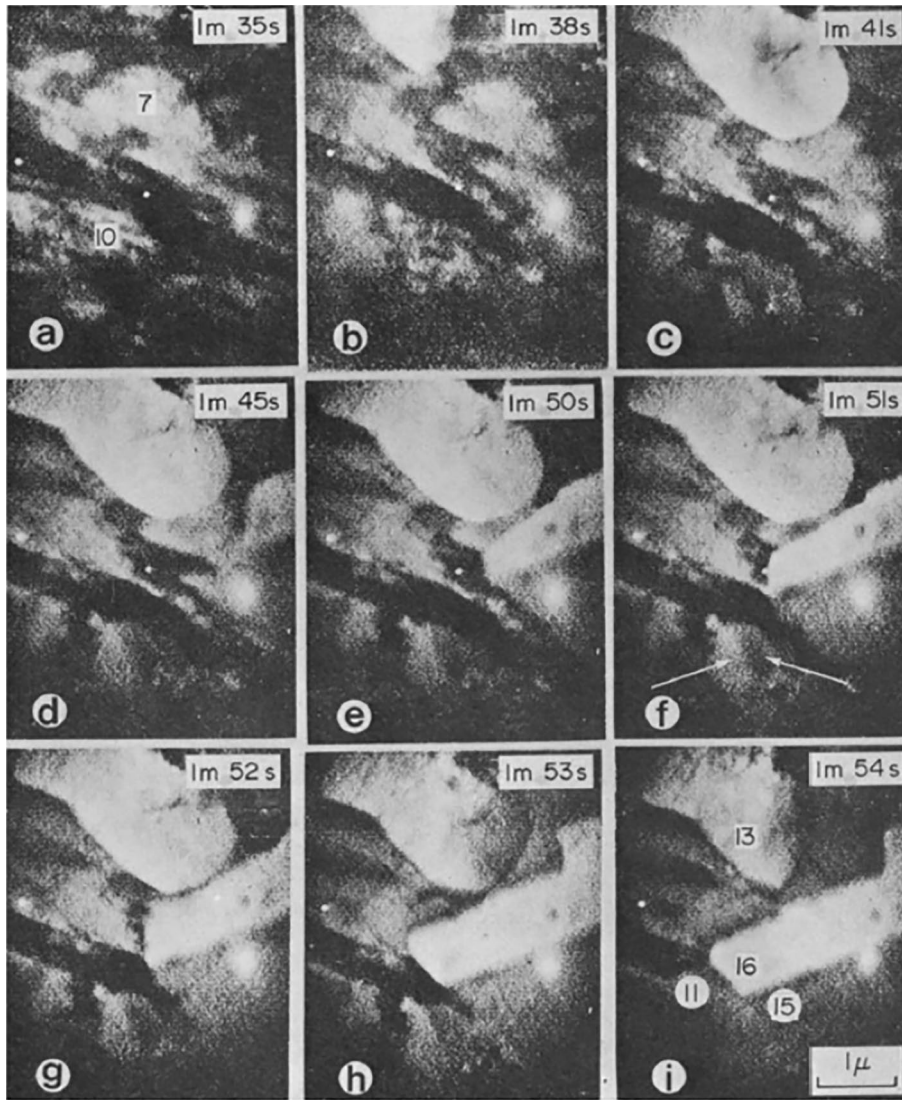


Figure 6: Recrystallization observation at different time steps in the copper using in situ high voltage transmission electron microscopy⁶¹.

using in situ TEM (Fig. 7). In situ experiments in a TEM have come a long way since then with indentation, environment control, tensile and compression testing and even dynamic deformation being performed in a TEM. With the advancement in sample preparation using focused ion beam milling, micro and nano pillar compression test as well as tensile test of different class has been successfully performed in situ in a TEM. The biggest advantage of TEM is that it can offer a high spatial-temporal resolution of defects like dislocations which act as major carriers of plasticity. Significant work on size-dependent plasticity that captures extrinsic effects like the sample size as well as intrinsic parameters like grain size and dislocation density has been captured using in situ

TEM. In one of the most seminal investigations of the twenty-first century, Shan et al.⁶³ showed the existence of mechanical annealing in nanopillar of nickel followed with near theoretical strength in the dislocation free micropillar, which was attributed to nucleation of dislocations as shown in Fig. 8. This phenomenon of limited source plasticity contributing to near theoretical shear strength has been a cornerstone in the mechanical behaviour of materials. Similarly, observation of grain boundary coalescence-induced grain growth in nanocrystalline nickel has shed light on the deformation mechanisms of nanocrystalline materials. The ability to perform an in situ tensile test in a TEM has provided valuable information on operative deformation mechanisms in a wide

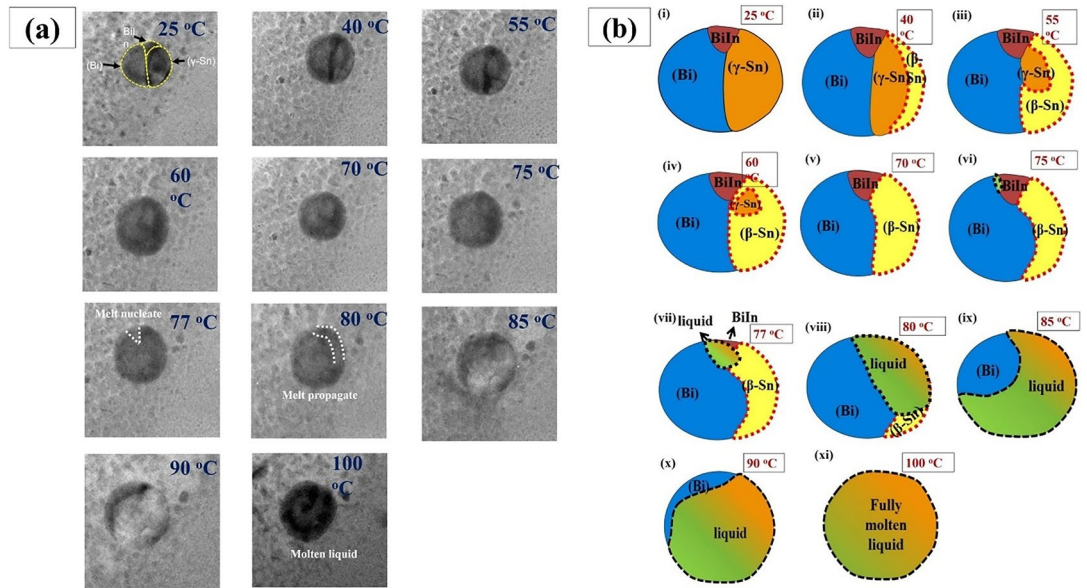


Figure 7: **a** In situ TEM images is showing the sequence of melting phase of nano particles of tri-phasic Bi-In-Sn alloys and **b** corresponding schematic⁴².

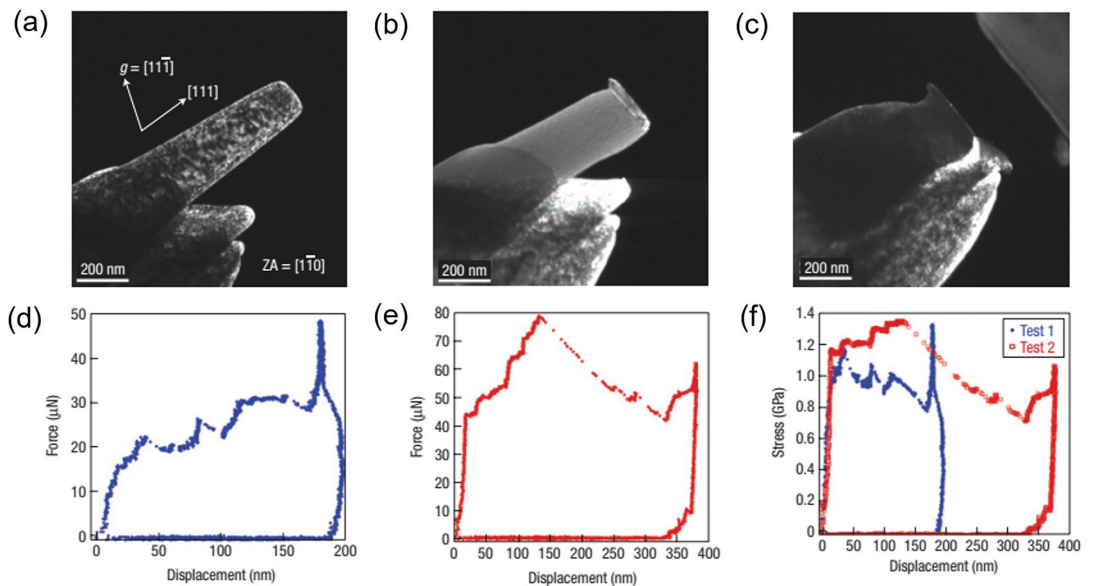


Figure 8: Dark-field TEM images of FIB micro-fabricated Ni pillar **a** with dislocations, **b** on deformation dislocations getting annihilated, **c** further deformation of same pillar having dislocations. Force–displacement curve of **d** first deformation and **e** second deformation. **f** Stress-displacement curve of both tests⁴³.

variety of materials and the ability to perform high strain rate deformation has shed light on dislocation dynamics that have helped develop better models for strengthening and strain hardening to predict the deformation behaviour of crystalline materials. The tensile sample preparation of the Cu is shown in Fig. 9. Recent efforts are focused

on controlling the environment so as to study the effect of hydrogen or corrosive environments on dislocation activity using in situ TEM experiments. It is expected that these platforms will offer better insight into unravelling the mechanisms of deformation in extreme environments in the near future.

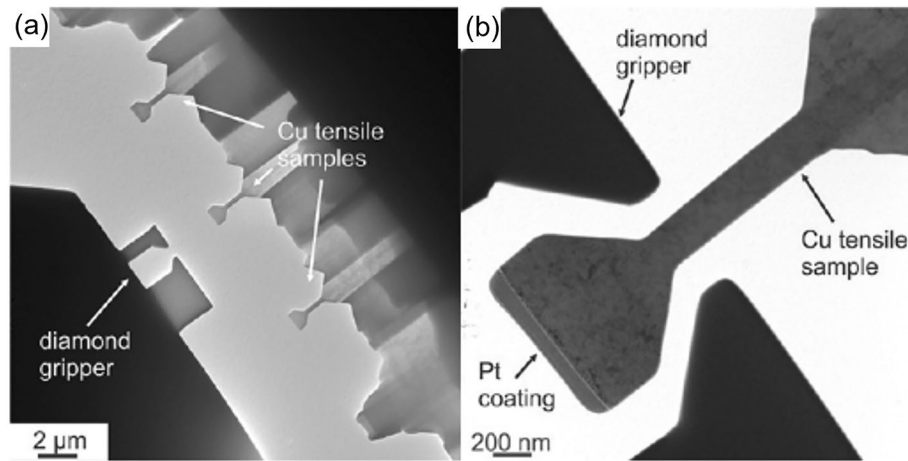


Figure 9: **a** TEM image of copper tensile samples at low magnification with diamond gripper and **b** single tensile sample with diamond gripper at higher magnification⁶³.

4.3 X-Ray Based Techniques Including Lab and Synchrotron Source

In addition to microscopic techniques that provide high spatial resolution, diffraction techniques using radiation like X-rays, synchrotron and neutron offer excellent angular resolution and provide valuable information of the reciprocal space that can be utilized for detailed defect characterization in crystalline materials^{50,55,64}. With the advent of imaging techniques like tomography and a combination of diffraction and tomography, it has been possible to link the spatial and temporal evolution of defects in the microstructure^{52–54,65}. Simple in situ experiments on diffraction techniques include heating and cooling stages in laboratory X-ray diffractometers that provide information on phase evolution as a function of temperature^{66–68}. The setup of the different combinations of tensile, EBSD with a high-energy X-ray source is schematically shown in Fig. 10. Similar experiments at a synchrotron source like the one at RRCAT Indore can provide real-time information on phase change by the use of ultrafast detectors and more importantly very high flux of x-rays. Third-generation synchrotron sources have made it possible to obtain a high flux of hard x-rays focused below 100 nm size, which provides high spatial resolution making not only heating and cooling experiments but also deformation experiments on conventional samples as well as low dimensional samples of micro-pillars or microspheres to offer deeper insights into length scale effects on mechanical behaviour^{55,68–71}. Synchrotron diffraction offers information in the reciprocal space unlike real space in microscopy techniques and therefore, it

is important to deconvolute the reciprocal space information to determine the microstructure and defect structure of the material under investigation. Techniques similar to that of line profile analysis of x-ray diffraction by whole profile fitting or moment method as well as that for reciprocal space mapping for thin film analysis can be applied in synchrotron diffraction. Synchrotron diffraction can provide localised information of structure, texture, defect structure in terms of dislocation density and twin probability in metallic materials with great accuracy^{44,60,68,72}. The presence of a high-intensity x-ray beam with a smaller size offers a unique tool to study fundamental deformation processes in small length scale testing shedding light on intrinsic length-scale effects in metallic materials as well as studying deformation heterogeneity in conventional testing. The ability to obtain additional information like chemistry from fluorescence or imaging from tomography offer multidimensional data for in situ synchrotron experiments. X-ray tomography using synchrotron radiation offers a unique tool to obtain real-time data on damage initiation leading to final failure in metallic materials due to the higher acquisition rate. The advent of diffraction contrast tomography has made it possible to obtain orientation information of different grains in the microstructure to achieve a real three-dimensional representation of the microstructure in real-time^{52,54}. This technique is in the development stage and is of great interest to the computational crystal plasticity community as it offers real-time monitoring of a representative volume element. In this regard, a high-energy synchrotron diffraction technique that does not

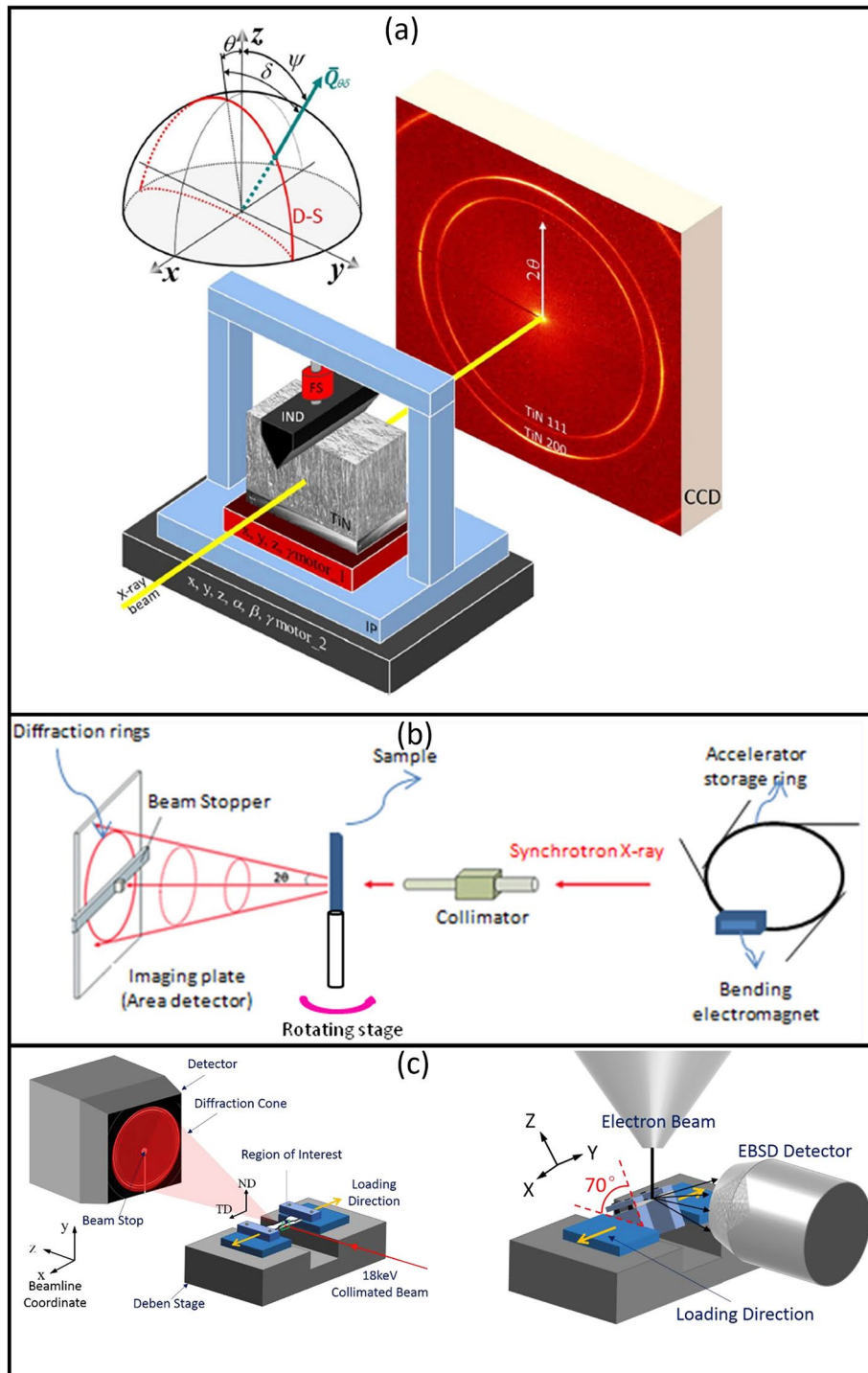


Figure 10: In situ synchrotron stages for different testing conditions. **a** Schematic of in situ nano diffraction setup, **b** schematic of normal stage diffraction setup and **c** schematic of combined in situ synchrotron and in situ EBSD diffraction setup [60-61](#).

focus on imaging but relies on obtaining information about a statistical representative volume element by indexing Laue diffraction spots from different grains in the microstructure is extremely

useful. The aforementioned in situ diffraction tools are generating a lot of interest due to their ability to feed into the crystal plasticity model and truly fit the ICME framework. One of the

major challenges for deriving useful information from in situ synchrotron diffraction methods is the complexity of data analysis and difficulty in the availability of access to different beamlines to perform some niche experiments. This is particularly true for a country like India that does not have a third-generation synchrotron source but judicious collaboration with the best synchrotron facilities and allotment of beamlines based on merit-based proposals have made the sophisticated technique available to the Indian research community.

4.4 Neutron

Neutron diffraction works on a similar principle as that of x-ray diffraction but neutrons as a probe offer additional advantages to detect lighter elements and isotopes as well as provide valuable information about the magnetic properties of the material⁵⁶. Neutrons are alpha particles produced by a nuclear reactor by fission of a radioactive material or from a spallation source. They interact weakly with an atom giving a very good signal-to-noise ratio. Since the interaction of neutrons is with that of the nucleus, they have higher penetration depth in metallic materials and are used to determine texture as well as residual stress in actual metallic components with coarse grain size^{73,74}. In addition, though neutrons are uncharged, they carry a spin and can interact with magnetic moments including those arising from the electron cloud of an atom, thus revealing the magnetic structure of a material. Similarly, the neutron cross-section of different elements is not in order of their atomic number like the x-ray scattering cross-section. It makes it possible to detect very light and very heavy elements and isotopes simultaneously using neutron diffraction⁵⁶. In situ experiments using neutron diffraction have focused on determining the evolution of texture and residual stress as a function of deformation and phase transformation but defect analysis including dislocation density and stacking fault probability can also be performed using neutron diffraction⁷⁵⁻⁷⁷. Recent investigations on the in situ performance of hydrogen fuel cells or lithium-ion batteries have exploited the ability of neutron to detect light elements like hydrogen, oxygen and lithium in the presence of heavier structural elements⁷⁸. Despite the tremendous opportunities with neutron diffraction, their use is limited due to difficulty in accessing these facilities across the world but some very fundamental and interesting insights on different materials have been observed over the years.

4.5 Combinatorial In Situ Experimentation

There is a strong desire to perform combinatorial or sequential in situ experiments to obtain better information on processes as they happen. One of the simplest examples is using multiple detectors in synchrotron diffraction or performing sequential micro-Laue diffraction and in situ SEM. In situ experiments can be followed with conventional characterization in steps to obtain a higher level of information that can shed better light on the operative mechanisms⁶⁹.

5 Contribution to ICME-MGI Framework

One of the missing aspects has been the implementation of well-developed computational tools employing multiscale simulations across length and time scales to develop a fundamental understanding of deformation, recrystallization, phase transformation or failure processes. It is envisioned that high-throughput in situ experiments should also be coupled with modelling and simulations to develop physics-based models that can help in reducing time for the development of new materials and processes. This is particularly important for the development of complex concentrated alloys which offer a wide composition space that would be impossible to probe in the conventional manner as well as a large number of process parameters for additive manufacturing^{21,40,79}. In addition, the failure of metallic materials is an interesting topic and capturing the same using in situ experiments is a challenge. Efforts need to be directed to develop statistical models which capture the physics of different processes so that failure can be predicted. Thus, combinatorial in situ experiments coupled with computational modelling should help us establish the journey of new materials from not the proverbial cradle to grave but also their reincarnation, which is necessary for sustainable materials development.

6 In Situ Experiments in Materials and Process Development

Metallic materials research has focused on developing materials for light-weighting to achieve high specific modulus, strength and fracture toughness as well as optimum performance in harsh working conditions of high temperature, corrosive environment or both since the industrial revolution. Recently the development of high entropy alloys or the complex concentrated alloys has challenged the traditional alloy design concept and has gathered a lot of attention of the metallurgical community due to the

vast compositional space offered by these alloys, which are also expected to offer access to hitherto inaccessible property space. The family of high entropy alloys or complex concentrated alloys has grown with the basic concept of 100% solute alloys to include many sub systems like medium entropy alloys and equimolar or non-equimolar multi-principal element alloys which offer a vast compositional space to be probed. The exploration of these new alloy systems using computational tools like first-principles calculations, thermodynamic modelling and recent use of machine learning needs to be complimented with high throughput in situ experiments to focus on the operative micro-mechanisms to enable physics-driven development of new alloys. Similarly, additive manufacturing of metallic materials using selective laser melting, direct energy deposition and electron beam melting has provided unique microstructures which were not accessible by conventional processing thus offering access to gaps in the property space for the existing alloys^{26,39,40,80}. The process parameter optimization for different additive manufacturing techniques like the power of the power sources (laser or electron beam), spot size, scan speed and scan strategy all play an important role in determining the evolution of microstructure and thereby govern properties of the additive manufactured components. In the process development for additive manufacturing too, in situ characterization plays an important role in the rapid development of processes to achieve microstructures of choice to yield desired properties. In the following two subsections, we will highlight the use of in situ characterization for the development of high entropy or complex concentrated alloys as well as additive manufacturing of metallic materials.

6.1 Complex Concentrated Alloys

Design and development of alloys over the last few thousand years has evolved from a serendipitous trial and error based method to a robust scientific method based on the sound principles of thermodynamics, kinetics and physical metallurgy guided by sophisticated experimental and computational tools in the last few decades^{81,82}. Nevertheless, the basic concept of an alloy as a combination of one of two base metals had stayed for eons till another fortuitous development of the so-called high entropy alloys by Yeh and Cantor^{83,84}. High entropy alloys defined as alloys of five or more elements in equal or near-equal proportions or the alloys with configurational entropy greater than $1.5R$,

where R is the universal gas constant led to tremendous interest in developing single-phase concentrated alloys for different applications⁸⁵. The excellent properties of the very first high entropy alloy, the CoCrFeMnNi Cantor alloy rekindled interest in alloy development and over the years the high entropy alloys have reincarnated in complex concentrated alloys with three or more elements with a combination of traditional mechanisms of strengthening and strain hardening to broaden the property space and garner interest in this class of materials^{41,72,86–92}. In situ experimentation has played an important role in the development of the complex concentrated alloys by rapid prototyping and the use of different in situ tools will be presented in this section.

6.1.1 In Situ XRD

In the search for new FCC single-phase equiatomic high entropy alloy compositions, Tazuddin et al.²³ carried out a systematic study of 1287 alloy compositions of 13 transition metals to develop the CoCuFeMnNi HEA by thermodynamic modelling using the CALPHAD tool. Sonkusare et al.⁴⁵ studied phase transformation in single-phase equiatomic CoCuFeMnNi complex concentrated alloy (CCA) using in situ high-temperature X-ray diffraction technique. It was observed that the metastable FCC α phase (lattice parameter = 0.361 nm) at room temperature decomposes into FeCo-rich β and Cu-rich γ phases at higher temperatures (Fig. 11). β phase ($a = 0.28$ nm) forms at 923 K, followed by γ phase ($a = 0.362$ nm) at 1123 K, leading to a microstructure with one BCC and two FCC phases. Atom probe tomography of CoCuFeMnNi CCA showed the presence of Cu-rich nano clusters, which segregated preferentially at the grain boundaries when the temperature was increased, hence forming the γ phase at the grain boundary. At 923 K, Fe and Co precipitated out from the α grains and formed the β phase. The transformation in this CCA was due to nucleation and growth mechanism and is similar to diffusion-induced grain boundary migration.

6.1.2 In Situ SEM

The tensile deformation behaviour of CoCuFeMnNi CCA was studied using in situ SEM. Figure 12 shows microscopic features in a few selected SEM images from a series of consecutive images acquired during the tensile test at small

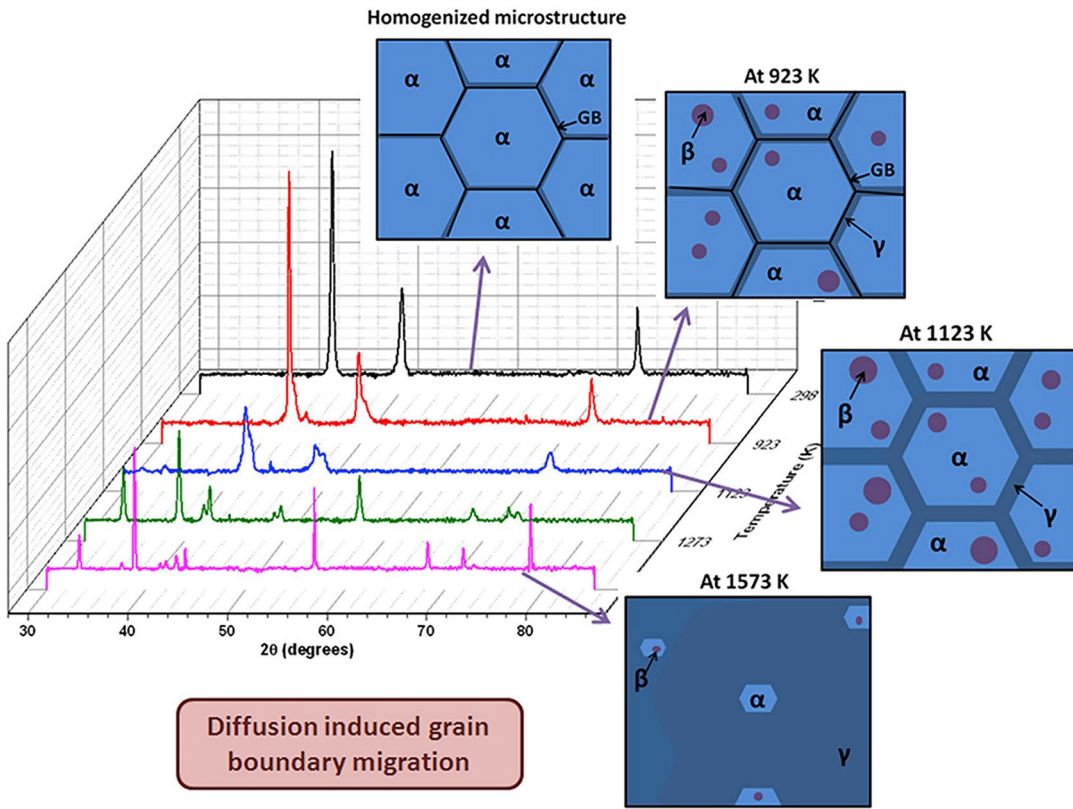


Figure 11: X-ray diffraction patterns for CoCuFeMnNi CCA at different temperatures, obtained from in situ high temperature XRD, along with schematic of microstructure to show phase evolution.

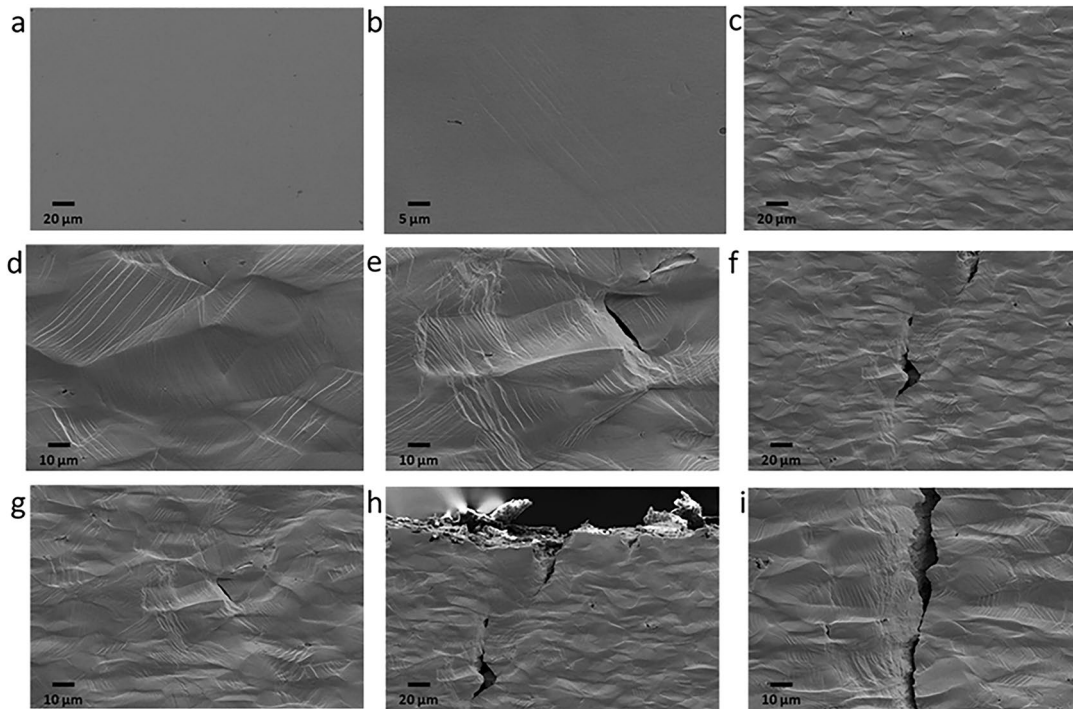


Figure 12: In situ SEM images of CoCuFeMnNi CCA during tensile test.

time intervals. The initial homogenized microstructure shows a single phase with few pores (Fig. 12a). During the tensile test, a few slip lines started to appear due to dislocation motion inside the grains and then the surface became rough. The grains became elongated, and now slip lines can be seen in all the grains (Fig. 12d), followed by the formation of shear lips at an angle of 45° (Fig. 12f). The crack formed due to the shear lips propagated and finally led to the fracture of the tensile sample (Fig. 12i).

6.1.3 In Situ EBSD

Ghassemali et al.⁹³ studied the effect of phase distribution on crack propagation in dual-phase AlCoCrFeNi CCA during tensile loading, using in situ EBSD (Fig. 13). The homogenized alloy

consisted of AlNi-rich BCC phase ($\sim 79\%$) grains and FeCr-rich FCC ($\sim 21\%$) phase was present as particles inside the grains as well as at the grain boundaries (Fig. 13c). During the in situ tensile deformation, crack nucleated at the triple junction of BCC grains and propagated transgranularly. The FCC phase at the grain boundaries acted as an obstacle and hence most cracks branched into new cracks, redirected, or even stopped as schematically shown in Fig. 13d. This shows the strengthening effect of the FCC precipitates at the BCC grain boundary.

The AlCoCrFeNi CCA was then subjected to a tensile test at intermediate temperature (550°C) and microstructure was observed using in situ EBSD⁸⁸. EBSD analysis near the fractured area revealed an increase in the amount of FCC phase

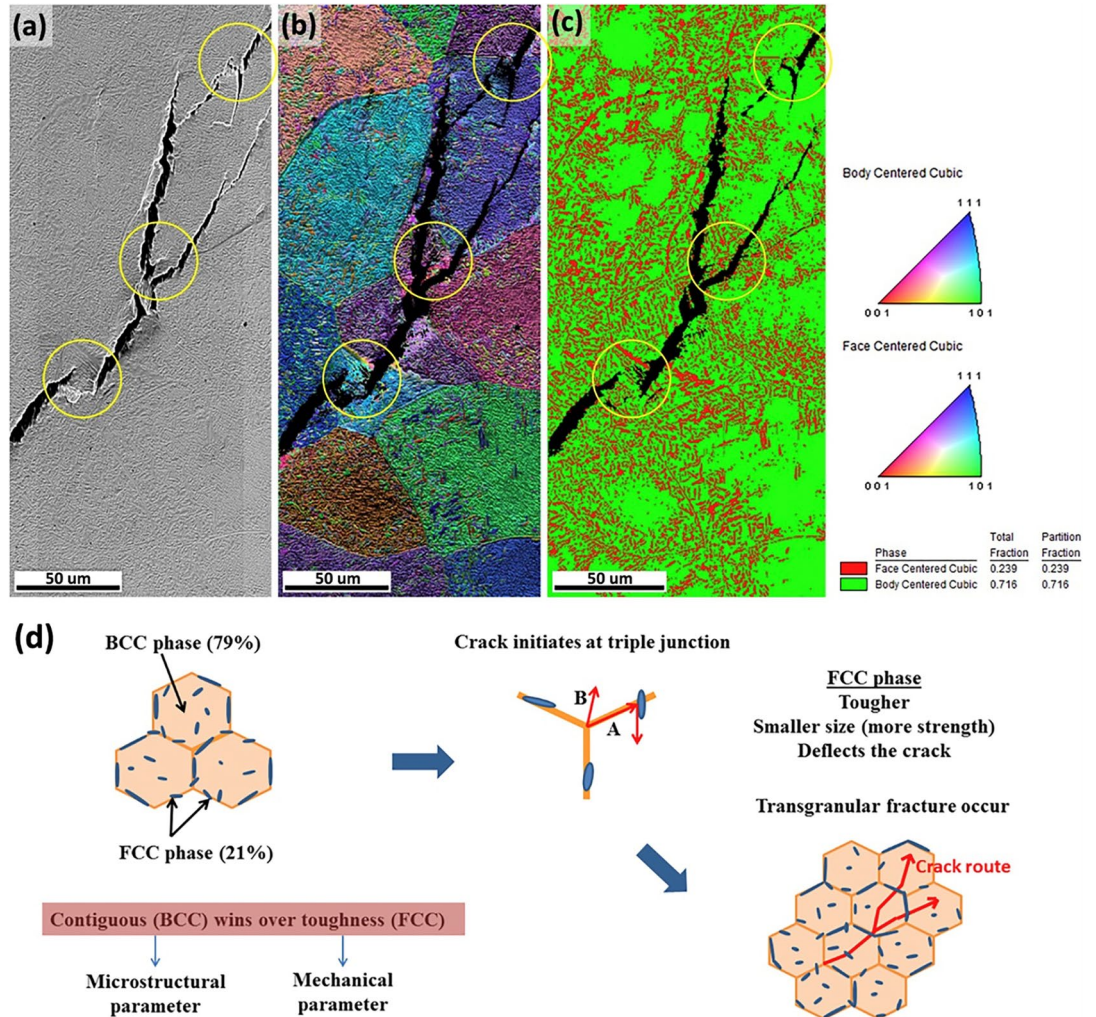


Figure 13: a SEM image, b inverse pole figure (IPF) map and a phase map of dual phase AlCoCrFeNi CCA. d Schematic to show crack initiation and propagation during tensile deformation of the alloy⁹³.

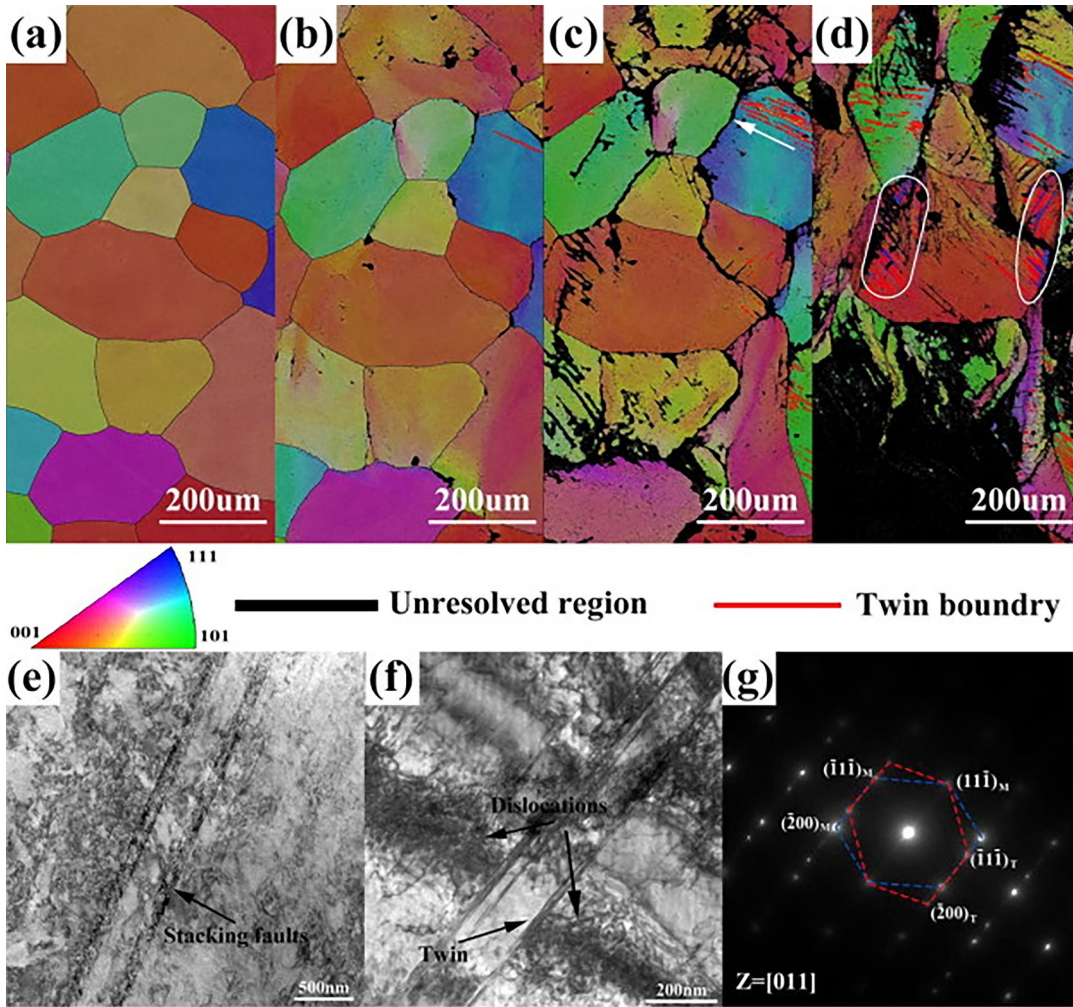


Figure 14: Inverse pole figure of C and Si doped FeMnCoCr CCA under tensile strain of **a** 5%, **b** 15%, **c** 30%, **d** necking. Bright field TEM images of **e** stacking faults at 5% strain and **f** twins at 15% strain, **g** selected electron diffraction of twins⁹⁴.

locally, suggesting dynamic precipitation of FCC phase. The new FCC phase showed no orientation relationship with the BCC phase indicating that precipitation was defect driven and not orientation driven.

Yang et al.⁹⁴ studied the microstructural evolution of C and Si-doped FeMnCoCr CCA subjected to different tensile strains, using quasi in situ EBSD. It was observed that microstructure does not change much at a strain of 5% and few twins form locally at a further strain of 15%, as shown in Fig. 14. When strain further increased, the grains started to stretch, refine and rotate and the number of twins increased, preferentially in the grains with $\langle 111 \rangle$ and $\langle 110 \rangle$ orientations. TEM images showed stacking faults at strain 5%, which led to deformation twin formation. These twins were observed to block the dislocation slip

and thus improving the work hardening of the alloy.

6.1.4 In Situ Synchrotron

Ma et al.⁷⁰ utilized in situ synchrotron to investigate tensile deformation behaviour of $Al_{0.6}CoCrFeNi$ CCA, consisting of FCC, BCC and σ phases. During the tensile deformation, it was observed that the FCC phase yielded before the BCC phase, and the latter carried more stress even with less volume fraction. In addition, a deformation-induced martensitic transformation from BCC to orthorhombic phase, was observed during the tensile deformation, in the grains with an orientation of B-[001]//loading direction and B-[110]//transverse direction. In the case of cyclic loading, the martensitic phase formed during the plastic deformation stage in the first loading, and

during the elastic deformation stage in the second loading.

Xu et al.⁹⁵ investigated the tensile deformation behaviour of face-centered cubic (FCC) $\text{Fe}_{20}\text{Co}_{30}\text{Cr}_{25}\text{Ni}_{25}$ and $\text{Fe}_{20}\text{Co}_{30}\text{Cr}_{30}\text{Ni}_{20}$ CCAs using in situ synchrotron. TWIP effect was found in both the alloys, but TRIP effect was observed only in $\text{Fe}_{20}\text{Co}_{30}\text{Cr}_{30}\text{Ni}_{20}$ (critical stress of ~ 555 MPa), with orientation relationship between the martensitic ϵ phase and FCC γ matrix as $\{111\}_{\gamma} // (0001)_{\epsilon}$ and $\langle 110 \rangle_{\gamma} // [110]_{\epsilon}$. The combination of TWIP and TRIP effects in $\text{Fe}_{20}\text{Co}_{30}\text{Cr}_{30}\text{Ni}_{20}$ CCA led to a good combination of tensile strength and ductility and improved strain hardening behaviour (UTS: 864 ± 35 MPa, elongation: 0.627 ± 0.021) than $\text{Fe}_{20}\text{Co}_{30}\text{Cr}_{25}\text{Ni}_{25}$ CCA (UTS: 763 ± 27 MPa, elongation: 0.618 ± 0.016). TEM images showed high-density dislocations and dislocation pile ups at the grain boundaries, formation of dislocation walls and annealed twin boundaries (Fig. 15).

6.1.5 In Situ Neutron Diffraction

Wang et al.⁹⁶ investigated the deformation response of FeCoCrNi CCA at 293 and 77 K using in situ neutron diffraction. Neutron diffraction data were used to calculate lattice strains, stacking fault probability and dislocation density. The lattice strain (ϵ_{hkl}) during loading can be calculated using shift in the diffraction peak, via the following equation.

$$\epsilon_{hkl} = \frac{d_{hkl} - d_{hkl,0}}{d_{hkl,0}}$$

Here, d_{hkl} is the d-spacing from (hkl) reflection at a given load and $d_{hkl,0}$ is the d-spacing of the (hkl) reflection at zero load. It was observed that stacking fault energy decreased as the temperature was decreased (from 32.5 mJ/m² at 293 K to 13 mJ/m² at 77 K) and tendency to form stacking faults and deformation twins increased along with dynamic Hall Petch hardening and dislocation hardening, thereby improving the strength and ductility at cryogenic temperature.

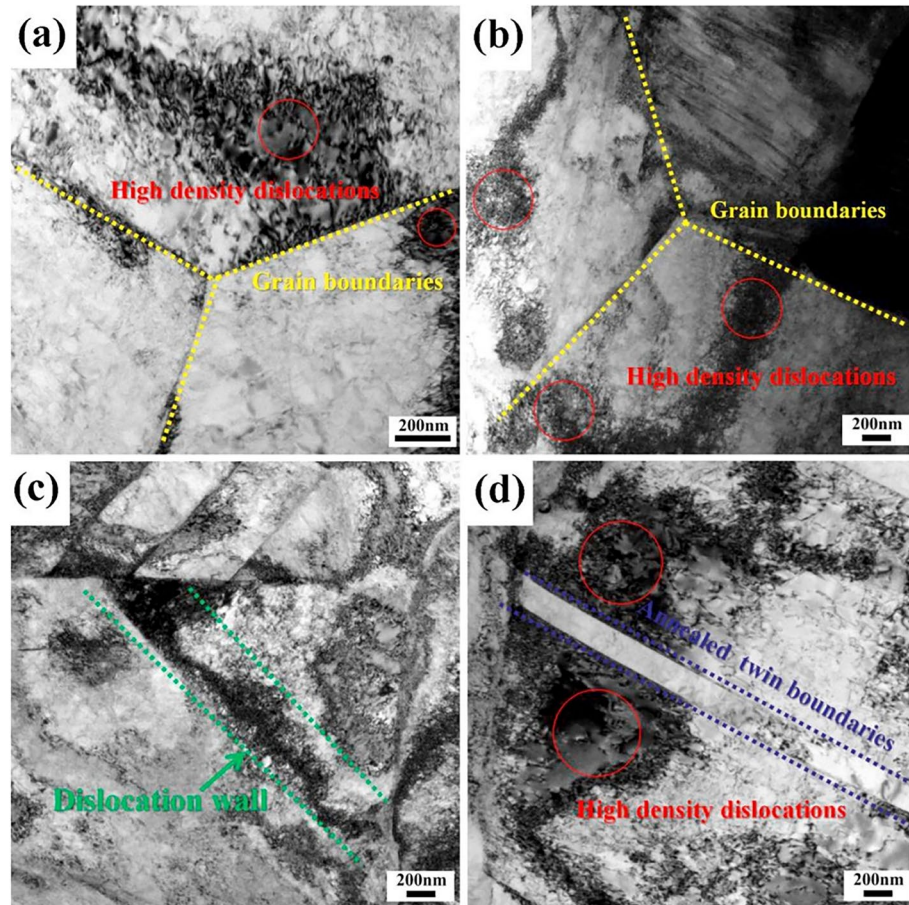


Figure 15: TEM images of deformed $\text{Fe}_{20}\text{Co}_{30}\text{Cr}_{25}\text{Ni}_{25}$ (a, c) and $\text{Fe}_{20}\text{Co}_{30}\text{Cr}_{30}\text{Ni}_{20}$ (b, d) CCA⁹⁵.

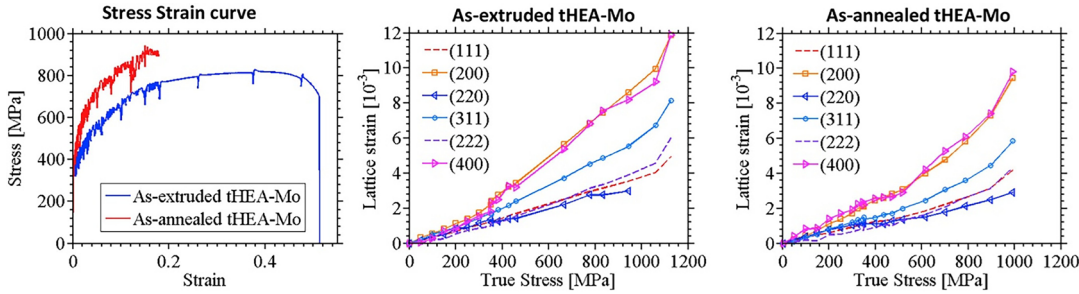


Figure 16: Stress strain curve and lattice strain evolution in as-annealed and as-extruded FeCoCrNiMo_{0.23} CCA⁹⁷.

Cai et al.⁹⁷ used in situ neutron diffraction along with electron microscopy to study deformation mechanism in hot extruded and annealed single-phase FCC FeCoCrNiMo_{0.23} CCA (Fig. 16). Mo addition increased the strength of the FeCoCrNi CCA because of solute solution strengthening. Evolution of lattice strain with respect to true stress showed two distinctive stages with varying slopes; (a) linear elastic loading and (b) linear plastic stage after a short transition from elastic to plastic. The (200) grains exhibited the lowest elastic modulus, followed by (311), (111) and (110) for as-extruded CCA. The elastic modulus of all grain orientations was found to be higher in annealed CCA than in as-extruded CCA, and slope of (200) grain was smaller in annealed CCA compared to as-extruded CCA, suggesting that (200) grains become harder after annealing. The as-extruded CCA showed stacking faults, twins and microbands due to low stacking fault energy (~ 19 mJ/m²) and hence high strength and ductility. Annealed sample was strengthened by Morich intermetallic particles, formed due to the decomposition of the alloy.

Wu et al.⁹⁸ studied the structural evolution of single-phase FCC FeCoNiCrMn CCA during tensile test using in situ neutron diffraction. The alloy showed strong elastic and plastic anisotropy and the evolution of lattice strains and textures in this CCA was found to be similar to conventional FCC metals and alloys. The deformation mechanism was found to be the operation of mixed dislocations. Fu et al.⁹⁹ studied the tensile deformation behaviour of Fe₅₀Mn₃₀Co₁₀Cr₁₀ transformation induced plasticity (TRIP) CCA, using real time in situ neutron diffraction and multiple mechanisms were found to be operative during the deformation in stages (Fig. 17). Stage one was the elastic deformation. The FCC to HCP transformation triggered at the yield point (~ 200 MPa) and hence stage two was TRIP along

with dislocation slip as the main accompanying mechanism. Stage three started at 400 MPa load when deformation twins started to nucleate in the HCP phase. Finally, stage four comprised of compression twinning and multiple twin systems along with TRIP and slip mechanisms. These multiple mechanisms in this CCA resulted in increase of ductility and work hardening potential of the alloy.

Naeem et al.¹⁰⁰ studied the evolution of different mechanisms during tensile deformation of Cr₂₀Mn₂₀Fe₂₀Co₂₀Ni₂₀, Cr₂₅Fe₂₅Co₂₅Ni₂₅ and Cr_{33.3}Co_{33.3}Ni_{33.3} CCA at 15 K, using in situ neutron diffraction experiments. A variety of mechanisms were observed at 15 K, starting from dislocation slip, followed by stacking faults and twinning, with the final transition to inhomogeneous deformation due to serrations, resulting in high work hardening. In situ neutron diffraction confirmed no phase transformation occurred during the tensile test.

Thus, it is clear that in situ characterization experiments using different probes have played an important role in rapid mechanism-based mechanistic development of complex concentrated alloys with excellent mechanical properties.

6.2 Additive Manufacturing

Additive manufacturing is a 3D printing processing technique of layer-by-layer deposition of a melt pool of powder and wire metals^{12,40,101,102}. It overcomes the manufacturing barrier of the conventional processing technique and helps to fabricate the intricate structure. Additive manufacturing offers design freedom, near-net or net-shape production, efficient use of materials in a short time with substantial cost-effective for many cases. Additive manufacturing uses many processing techniques i.e. selective laser melting, electron beam melting, laser metal deposition, ultrasonic additive manufacturing, gas metal arc

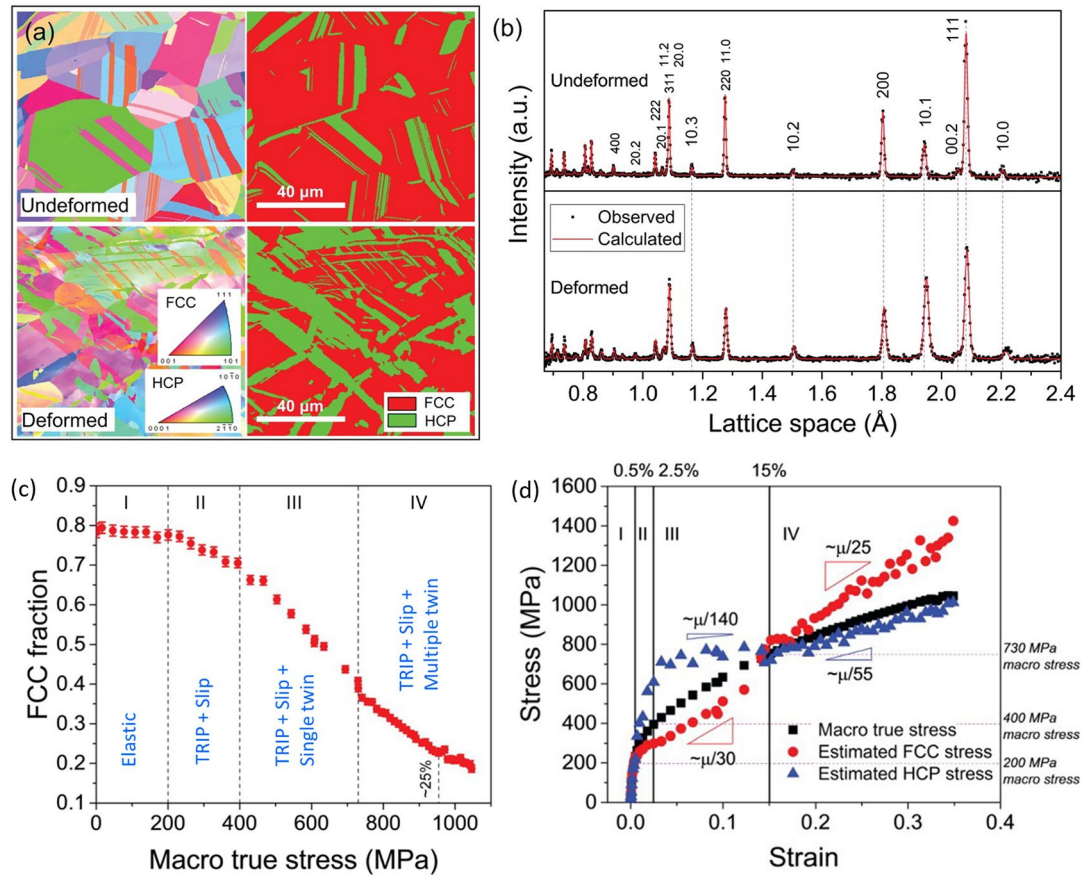


Figure 17: **a** EBSD inverse pole figures and corresponding phase maps and **b** neutron diffraction patterns in comparison with the Rietveld refinements before and after ~ 6% deformation. **c** Dynamic FCC fraction during tensile test, **d** Phase specific stress strain behaviour of Fe₅₀Mn₃₀Co₁₀Cr₁₀ CCA¹⁰¹.

weld, etc. A variety of metals and alloys i.e. copper, steels, titanium alloys, aluminum alloys, Ni alloys and high entropy alloys or complex concentrated alloys have been used to fabricate the final product. Unlike conventionally processed microstructure, additively manufactured microstructure consists of porosity, thermal residual stress and gradient microstructure depending on processing parameters. Therefore, to mitigate the porosity and the residual stress as well as understanding the effect of complex microstructure on the properties inclined the attention of many researchers. In situ techniques give a significant insight to recognize the hidden mystery of additive manufacturing processed alloys. Many studies were carried out to appreciate the processing-microstructure-properties paradigm. A brief summary and the importance of in-situ experiments are focused on the following sections.

6.2.1 Cyclic Phase Transformation

A layer-by-layer deposition offers a significant microstructural change due to remelting and cyclic heating of a layer by the upcoming layer in powder-based additive manufacturing processes. Jeremy et al.¹⁰³ studied the microstructural changes of X40CrMoV5-1 steel during deposition by laser metal deposition (LMD) using in situ synchrotron X-ray diffraction in transmission mode at the Deutsches Elektronen-Synchrotron (DESY) in Hamburg, Germany. A schematic and the photograph of the actual experimental setup for simultaneous deposition and synchrotron diffraction is provided in Fig. 18. A solid-state YAG laser having 1.4 μm wavelength, 300 W power, 0.3 mm spot size was used at a working distance of ~ 5 cm below the powder delivery nozzles. The detail of the metal deposition is given in Table 2. The deposition was performed on the same base metal (20 × 50 × 10 mm³) substrate clamped by a massive copper holder for sufficient heat flow. A sample of 30 × 1.5 × 6.5 mm³ was prepared by

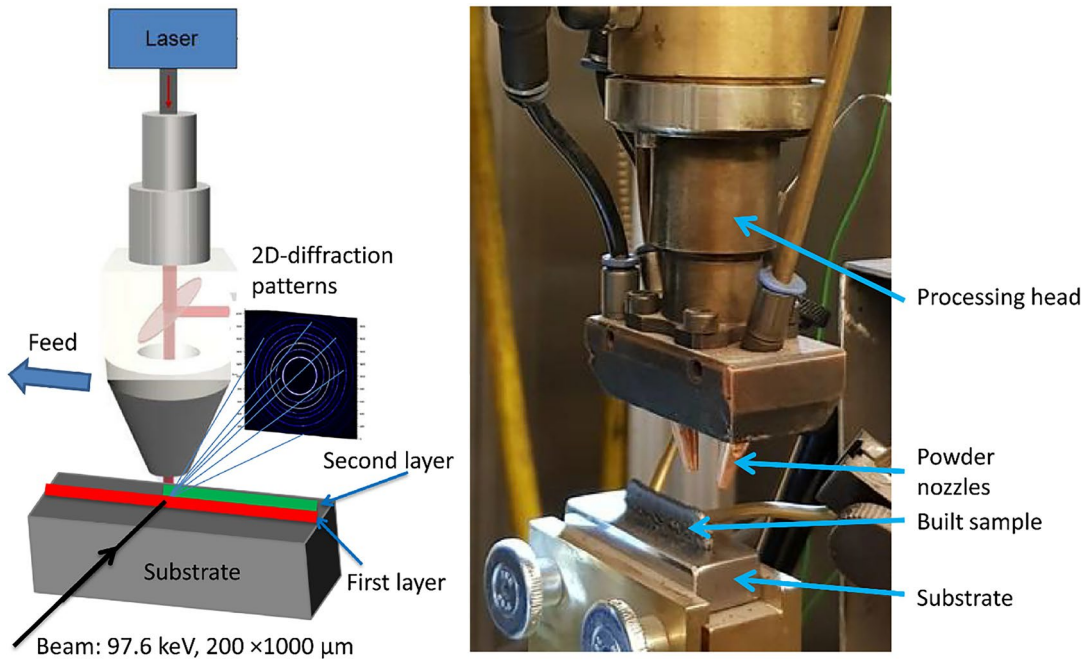


Figure 18: Experimental setup for in situ synchrotron XRD measurement during laser metal deposition (LMD) of steel X40CrMoV5-1. **a** Schematic of in situ XRD and LMD and **b** Image of the LMD process head and the built sample¹⁰³.

Table 2 The process parameters of laser metal deposition for printing of X40CrMoV5-1 steel¹⁰³.

Feed rate	Dwell time between each layer	Powder mass flow	Height position increment for each layer
300 m/min	5 s	5.6 g/min	0.3 mm

printing 30 successive layers exploiting two powder nozzles at 2.4 bar argon atmosphere.

A monochromatic synchrotron x-ray beam (97.6 keV) was used at a frequency of 10 HZ in transmission mode through the thickness of the sample. 2D Perkin-Elmer detector with 2048×2048 pixels was used to collect the diffraction pattern and was situated at 1.42 mm from the sample. A $1000 \times 200 \mu\text{m}^2$ cross-section of the synchrotron beam was focused on the first deposited layer just above the substrate in the course of the whole experiment. Heating rate up to 30,000 K/s or more was observed during metal deposition and subsequent cooling rate was in the range of 300–2000 K/s above 1273 K substrate temperature thereafter on further cooling, it reached 20 K/s cooling rate.

A set of 45 diffraction patterns were recorded from the first built layer during printing of the first layer and subsequent fast cooling of the second layer. The corresponding 3D integrated diffraction pattern is shown in Fig. 19a. In the initial three frames, the liquid phase was identified in the form of a broad low-intensity peak, followed by increasing sharp delta ferrite (BCC) peaks and then the austenite (FCC) peaks were observed. Further, delta ferrite peaks disappear within a few measurements and the intensity of the austenite peaks rapidly increase. An austenite to martensite transformation was observed after 12 frames (1.2 s) that continued for the subsequent cooling period.

Figure 19b represents the change in the amount of austenite and martensitic phase on the first built layer during the subsequent 11 deposited layers on the top. In this whole process, the thermal cycle on the first deposited layer continuously decreased and it was observed that remelting of the first layer occurred up to the third deposited layer on the top (Fig. 19c) and each time new martensitic transformation occurred due to full re-austenitizing. Further, partial re-austenitizing of the first layer was observed till 7 deposited layers on the top and its fraction continuously decreased due to a continuous decrease in the thermal cycle. For the next deposited layer,

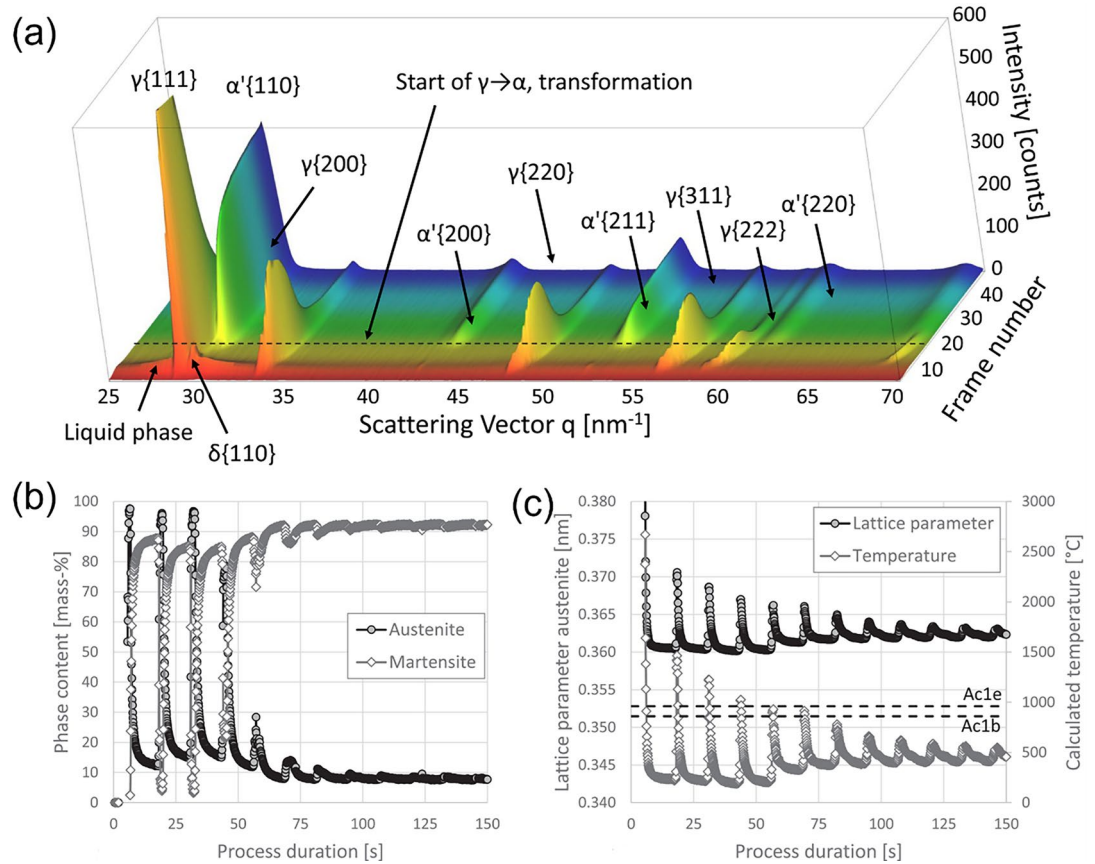


Figure 19: **a** 3D view of 45 integrated diffraction patterns recorded in the first layer during generation and cooling of the second built layer on top during the LMD process. **b** Evolution of phase contents as well as **c** austenite lattice parameter and calculated temperature in the first built layer during its generation and subsequent deposition of the next 11 layers on the top¹⁰³.

the maximum temperature was not sufficient to transform martensite to austenite and self-tempering was observed. Thus, in operando monitoring of phase evolution in additive manufacturing using synchrotron diffraction helps in controlling the process parameters like deposition rate and laser power to achieve desired phase fraction that determines the mechanical properties of the AM component.

6.2.2 Residual Stress

The main complication in the additively manufactured Ti6Al4V is the undesirable residual stress due to thermal cycles by melting and remelting in successive layer deposition¹⁰⁴ and martensite phase formation due to high cooling rate (SLM produces $\sim 10^3$ to 10^8 K/s¹⁰⁵ unlike conventionally process having 1.5×10^3 K/s on water quenching¹⁰⁶). These undesirable properties limit the application and numerous investigations were performed to design heat treatment conditions to obtain suitable phase fractions to

achieve desirable mechanical properties. In situ XRD heating and in situ TEM heating setup were employed to monitor the evolution of phases during heat treatment¹⁰⁷. Stress relaxation and phase decomposition were analysed by XRD with vacuum heating stage (Anton Paar DHS 1100 heating stage) in the range of 25–1000 °C. Micro/nano structural changes were investigated in the range of 298–1173 K using FEI Titan with 300 kV acceleration voltage with 4-point feed-back controlled heating based on a MEMS-based heating system.

Figure 20a-i shows in situ XRD plot at the fixed area for the different temperatures during heating. At room temperature, the asymmetric peaks indicated an imperfect lattice due to the presence of anisotropic lattice micro-strain, dislocation densities and crystallite size¹⁰⁸. On heating, XRD peaks sifted towards the left side and suggested the release of compressive residual stresses by an increase in lattice parameter and narrower peaks indicated an increase in the crystallite size

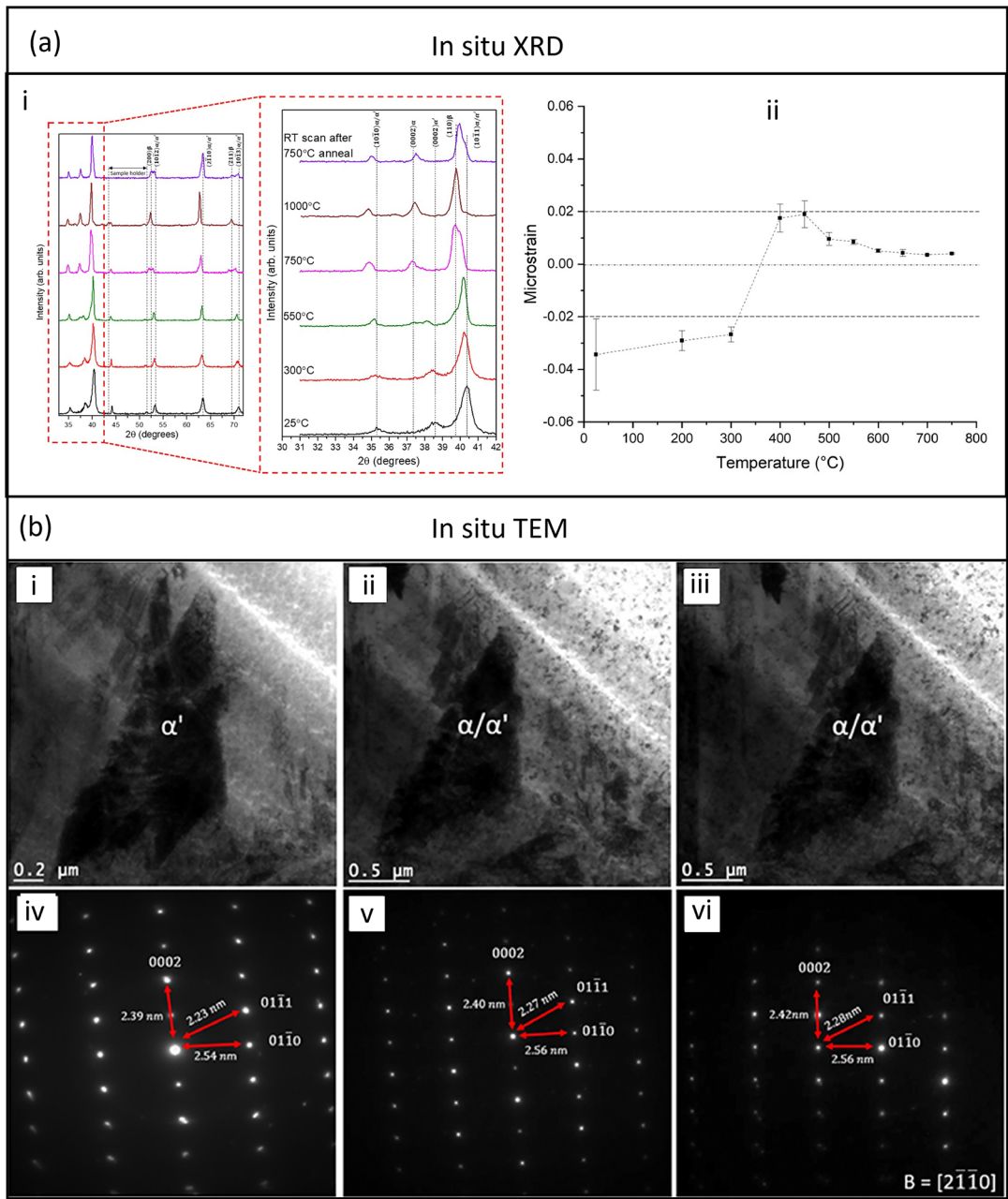


Figure 20: a-i In situ X-ray diffraction patterns and corresponding a-ii micro strain evolution were plotted during heating in the temperature range of 25–1000 °C for AM Ti6Al4V. b TEM bright field images acquire at (i) 25 °C, (ii) 550 °C and (iii) 600 °C and their respective diffraction patterns (iv–vi) for AM Ti6Al4V¹⁰⁷.

and reduction in the micro-strain. Micro-strain (values determined from peak shift) versus temperature plot (Fig. 20a-ii) suggested that initially microstructure had compressive stress upto 300 °C and after that it was slightly tensile. The stress relaxation was spotted in the range of 25 °C to 400 °C without martensitic phase transformation. At 550 °C from Fig. 20a-i, $(110)_{\beta}$ peak can be observed at the base of $(10\bar{1}1)_{\alpha/\alpha'}$ and the splitting of (0002) peak can be observed between 37°

and 38.6°. Thus, it indicated that martensite α' decomposed into equilibrium α and β phases and further at 750 °C, fully transformed α and β phase was observed. On further heating to 1000 °C showed that the intensity of the beta phase peaks increased at the expense of the equilibrium α phase peaks.

In situ TEM images and respective diffraction patterns for the temperature of 25 °C, 550 °C and 600 °C are represented in Fig. 20b. Diffraction

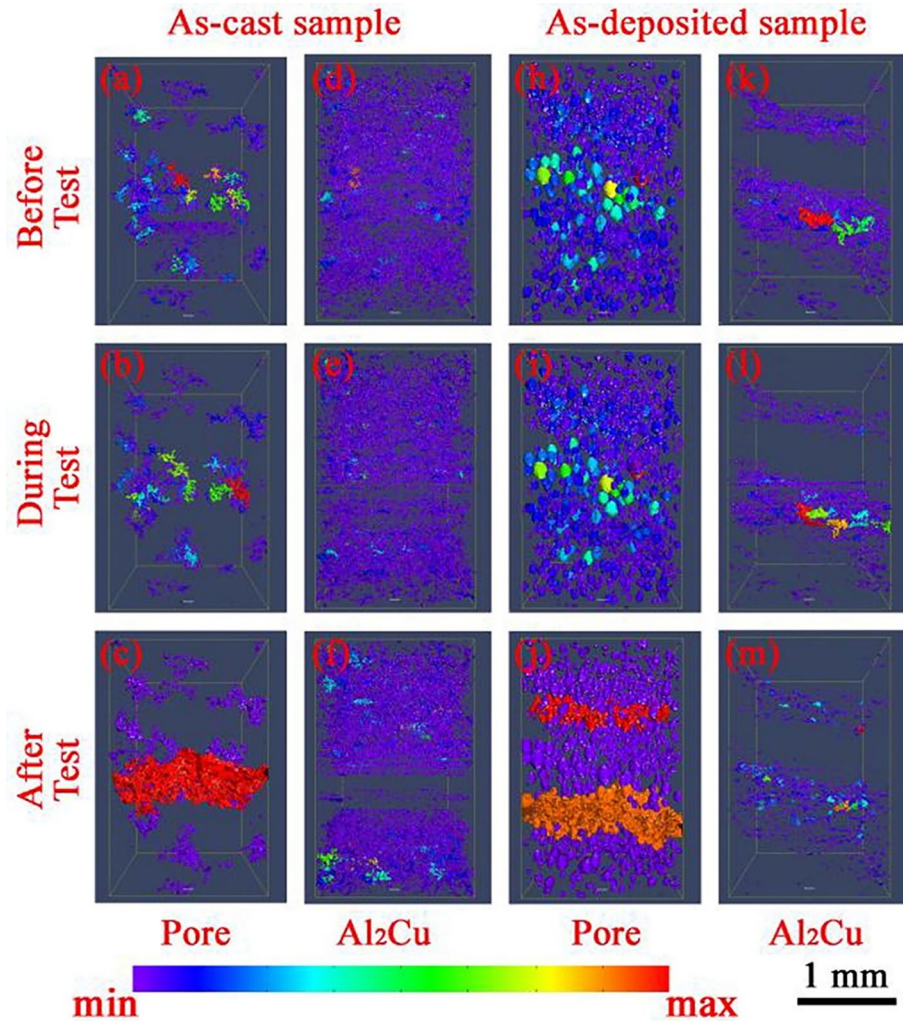


Figure 21: In situ XRM images show the distribution of pores for **a–c** as-cast and **g–i** as-deposited. Distribution of precipitates Al_2Cu for **d–f** as-cast and **j–l** as-deposited during tensile testing of 205A aluminium alloy¹⁰⁹.

patterns showed the significant change in the relative d-spacing of (0002), (01 $\bar{1}$ 0) and (01 $\bar{1}$ 1) planes, which validated the stress relaxation and crystal structure changed with an increase in temperature.

6.2.3 Effect of Porosity

The evolution of the undesirable pores is a major issue in as-printed Al alloys. High porosity caused by trapped argon gas which is used for inert atmosphere along with hydrogen and oxygen gas from air and decomposition of water vapour. These pores worsen the ductility, although it achieved better strengthening and larger maximum stress than as-cast Al alloys³⁹. 3D X-ray microscopy (XRM) nicely showed the pores and precipitate Al_2Cu distribution, shape and size. In situ damage evolution was explicitly

studied using x-ray microscopy (XRM) (Xradia 520 Versa)¹⁰⁹. Figure 21 refers to the spatial distribution of the pores and Al_2Cu precipitate before test, during test and after test for as-cast and as-deposited Al alloy. As-deposited showed relatively higher and homogeneously distributed pores (3.51%) than as-cast having localised and interconnected pores (0.336%). A large amount and homogeneously distribution of Al_2Cu were clearly noticed in the as-cast aluminium alloy compared to as-deposited aluminium alloy having lesser and heterogeneous distribution due to very high cooling rate. As-cast sample failed at the area of localised pores and a lesser amount of Al_2Cu precipitates. However, the conventionally processed sample failed at the location of the larger in size and the higher

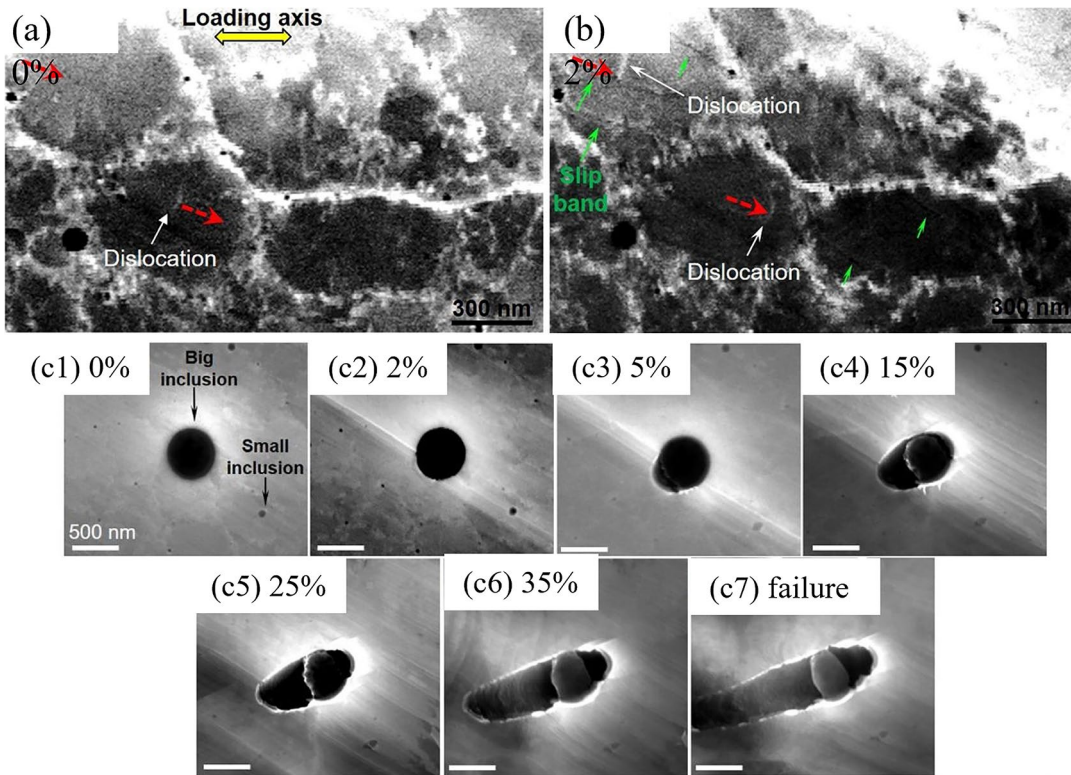


Figure 22: In situ electron channelling contrast images (ECCI) for **a** 0% and **b** 2% deformation step. In situ secondary electron images for the strain steps of **c1** 0%, **c2** 2%, **c3** 5%, **c4** 15%, **c5** 25%, **c6** 35% and **c7** failure in AM 316 stainless steel¹¹⁰.

number of pores as well as higher content of Al_2Cu precipitates.

6.2.4 Damage Micro-Mechanism Around Inclusion

Oxide inclusions form in additively manufactured 316 stainless (316 SS) steel due to gas impurity and native oxide layer on the outer surface of powder during deposition^{111–114}. These inclusions are oxides of Si, Mn and Ti due to their higher affinity towards oxygen than other alloying elements of 316 SS^{115,116} which contributed to a detrimental effect on the toughness despite the alloy showing good work hardening behaviour due to cell structure formation. Thus, a systematic damage micro-mechanism was needed to understand the causes of damage around the inclusions. In situ electron backscatter (EBSD) and electron channelling contrast imaging (ECCI) were used for characterization to understand the damage phenomenon¹¹⁰. ECCI image at 2% (Fig. 22b) refers to the motion of dislocations inside the cell as shown by a white arrow around a big inclusion

that also shows a slip band in the vicinity. Kong et al.¹¹⁰ observed the heterogeneous sub microcellular structure around big inclusion and dislocations first generated inside the large cellular structure due to lower CRSS value for slip. In situ secondary electron images shown in Fig. 22c1–c7 suggested an asymmetric crack growth around the inclusion with subsequent deformation. It was observed that crack initiation started at the interface of the slip band and inclusion due to high local stress after 2% deformation followed by growth aided by dislocation absorption-mechanism at the surface of the void. EBSD IPF map (Fig. 23a1) and ECCI image (Fig. 23a3) confirmed the deformation twin ahead of the crack tip after 15% deformation. Further at 25% deformation, the IPF map (Fig. 23b1) confirmed the twin thickening and the ECCI image (Fig. 23b2) indicated the nanotwin cluster which inhibited the further growth of the crack. The detailed damage micro-mechanism around the inclusion with increasing strain could be understood by the schematics shown in Fig. 23c1–c4.

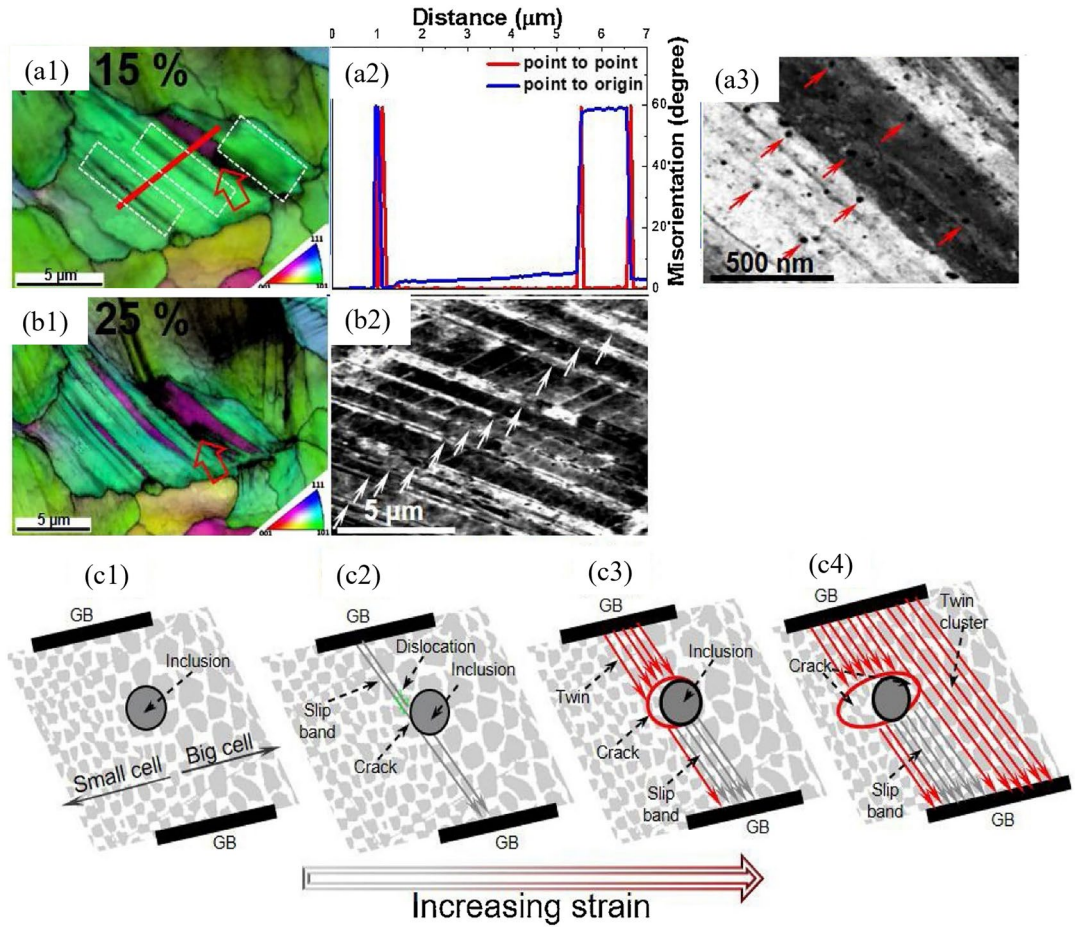


Figure 23: Inverse pole figure maps for 15% (a1) and 25% (b1). a2 Misorientation distribution along the red line. ECCI images for a3 15% and (b2) 25%. The schematics with the increasing strain levels are showing c1 initial stage, c2 slip band initiation and crack occurred near the inclusion, c3 nano twin initiation, c4 nano twin growth and crack propagated, respectively. The big inclusion sites are marked using big red arrows in (a1, a2, c1, c2)¹¹⁰.

6.2.5 Fracture Anisotropy Due to the Crystallographic and Spatial Orientation of α Lath

AM Ti6Al4V has $\alpha + \beta$ phase microstructure consisting of columnar prior beta grain morphology with preferential $\langle 100 \rangle$ crystallographic texture along the vertical direction (VD). Such morphology generates due to thermal gradient which prevents the nucleation ahead of solidification during metal deposition¹¹⁷⁻¹¹⁹. It has concentrated spatial orientation of alpha lath and crystallographic texture. The deformation and damage anisotropy due to columnar grain morphology, the crystallographic orientation and spatial orientation of alpha lamellae in Ti6Al4V is well established in the literature^{117,120-122}.

To understand this for additive manufactured Ti6Al4V, three different orientations of tensile samples along the vertical direction

(VD), at 45° to the horizontal direction (HD) and HD were prepared¹²³. An in situ SEM study was performed on the tensile stage inside the FE-SEM chamber for each case and images were captured for different deformation steps. Figure 24 refers to the load versus displacement curve as well SEM images at different displacement steps for HD sample. A band of slip lines along the alpha lath which is $\sim 45^\circ$ to the loading axis can be seen at the step of 600 μm . EBSD analysis suggests that alpha laths have a high Schmid factor for prismatic slip systems. On further deformation, a crack indicated by a black arrow grows along the alpha lath oriented at 45° to the loading axis. It suggests the crack is more prone to those laths which are oriented along the highest shear stress plane. When a crack encounters a lath, it resists crack

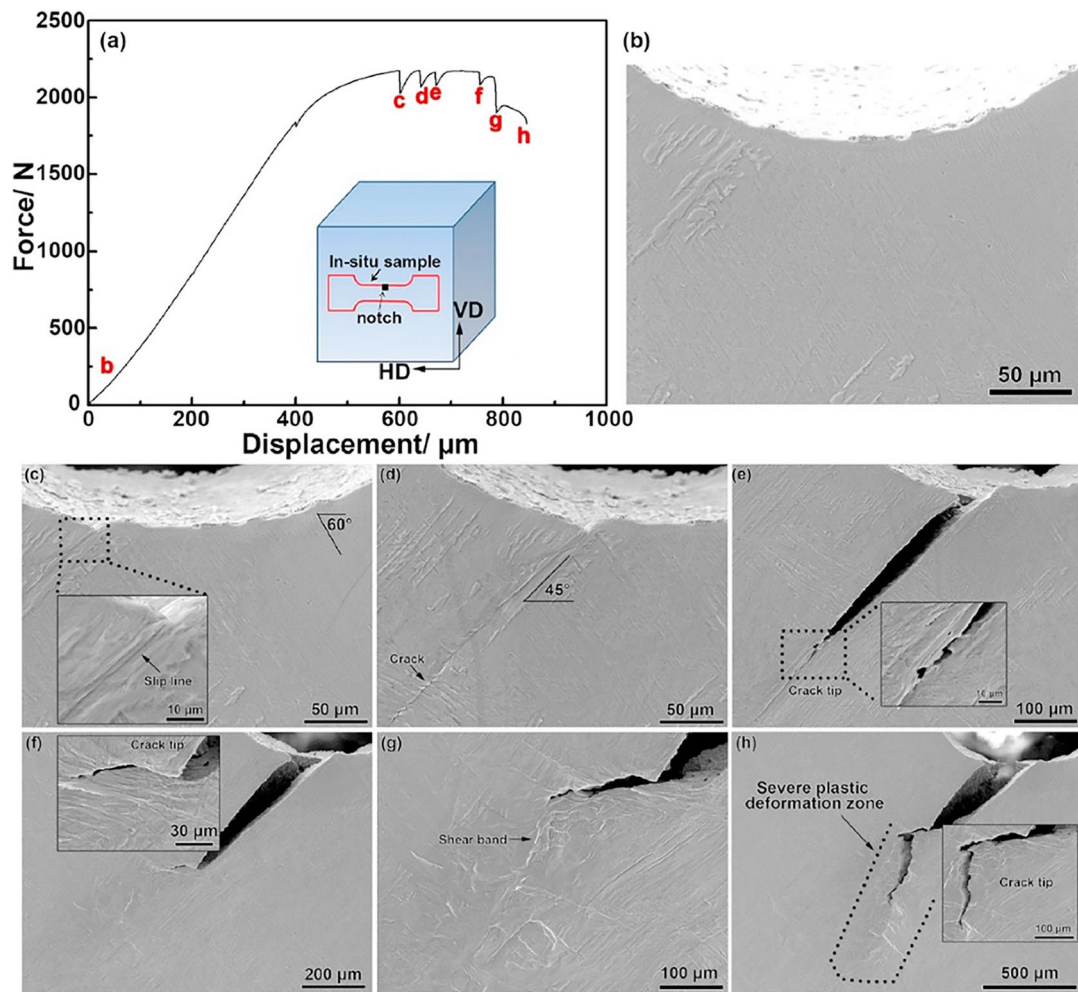


Figure 24: a Load–displacement graph of HD sample. Corresponding, in situ scanning electron images for the different deformation steps (b–h) of AM Ti6Al4V¹²³.

propagation by localized plastic deformation leading to the formation of a shear band which helps in further crack propagation as shown in Fig. 24g, h. Similarly, in situ studies of other orientations is also provided in the investigation¹²³. The sample loaded along HD showed lower maximum stress than the sample loaded along 45° to HD direction and the VD sample showed the lowest stress. This anisotropy in mechanical properties is mainly attributed to alpha laths rather than columnar prior beta grain boundaries. The sample loaded along the VD direction showed higher deformation till failure than the sample loaded along the 45° to the loading axis and the highest strain till failure was observed for the HD sample. The present investigation concluded that the morphological and crystallographic orientation of the alpha

laths determine the fracture anisotropy in AM Ti6Al4V alloy.

6.2.6 Hydrogen-Embrittlement

Hydrogen-embrittlement causes detrimental effect for steels due to the transition mode of failure from the ductile to brittle¹²⁴. Figure 25 indicates an in situ synchrotron x-ray diffraction study for hydrogen-free and hydrogen-charged AM maraging steel during a tensile test¹²⁵. It was observed that the intensity of retained austenite peaks for hydrogen-free maraging steel reduced with deformation and merged into the background (Fig. 25a). However, the hydrogen-charged specimen (Fig. 25b) did not show significant changes in the intensity of retained austenite peaks even after failure. The stress required for the transformation of retained austenite to martensite for hydrogen-charged specimen was

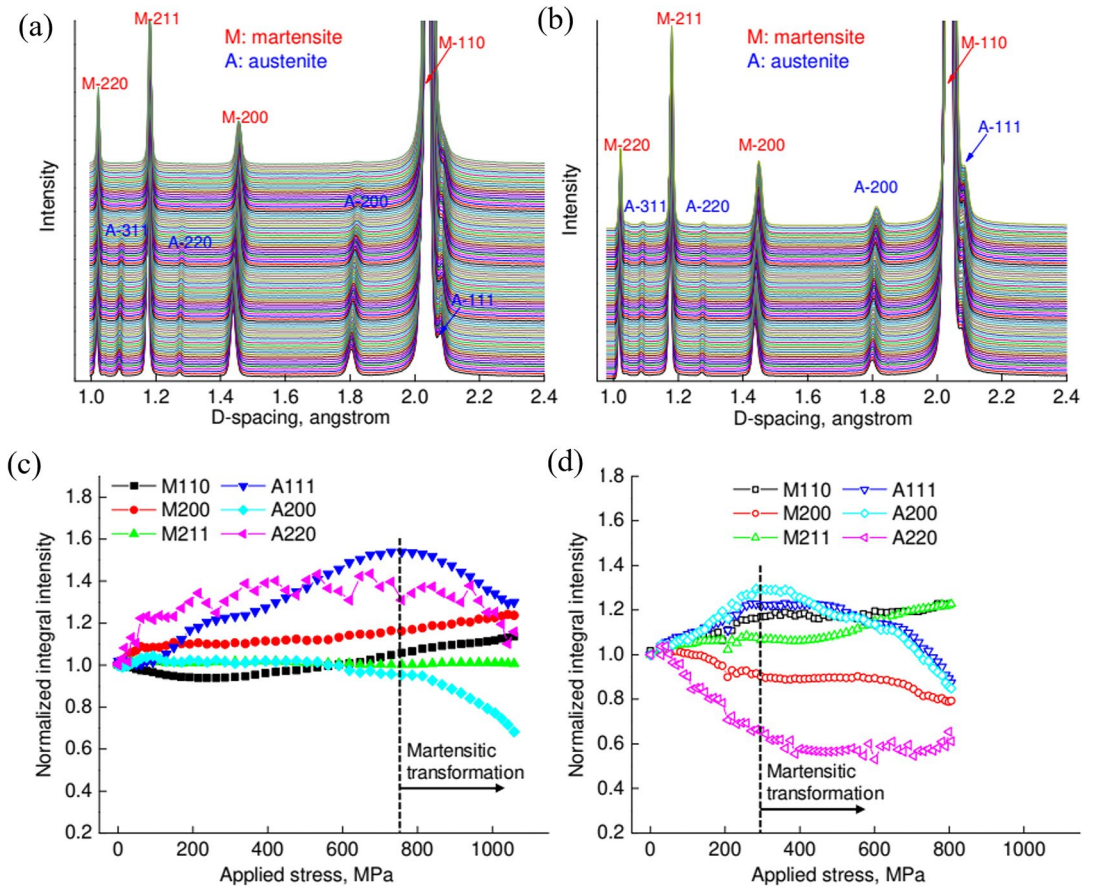


Figure 25: In situ synchrotron X-ray diffraction plots for **a** hydrogen free and **b** hydrogen charged samples. Corresponding, normalized integral intensity plots of retained austenite and martensite phase for **a** hydrogen free and **b** hydrogen charged AM maraging steel¹²⁵.

300 MPa which was lower than the required stress (760 MPa) for the hydrogen-free specimen (Fig. 25c, d). Thus, a premature transformation of martensite caused enhancement in localized stress; consequently, leading to a brittle fracture.

The representative studies covered in the present section clearly demonstrate the role of in situ characterization techniques for process parameter optimization, in service performance as well as failure in different operative conditions for additive manufactured metallic materials, thus highlighting the significant role of in situ techniques in process-property-performance paradigm in additive manufacturing.

7 Way Forward

A brief overview of the in situ characterization experiments as high throughput tools for materials and process development shows the tremendous potential of these tools for rapid development of materials and processes. With the vast compositional and process parameter space

available for exploring, it is more of a rejection process than a selection process with a desire to avoid false negatives. We are able to probe the real space for the evolution of grain structure, phase transformation and damage accumulation while compositional space can be explored at different length scale to determine the partitioning of elements at different length scales. Similarly, characterization tools providing a view of the reciprocal space offer information on the evolution of structure, texture, stress and strain in the material. Combinatorial approach with in situ multiple probes like synchrotron diffraction and fluorescence mapping coupled with SEM based in situ EBSD can offer information from the real, reciprocal and composition space at the same time. Thus, it is possible to obtain hyperdimensional information about the microstructure on the new platform and monitor it as a function of external stimuli. Combinatorial microscopy techniques like 3D diffraction contrast tomography offer a wide range of information to develop

a fundamental understanding of processes in 4 dimensions. The real attributes of the microstructure provide huge multidimensional data which can be used to generate knowledge using machine learning and artificial intelligence tools. It is envisioned that few high throughput in situ experiments will provide high-quality multidimensional information that can be used to predict properties and performance of materials based on physics-guided machine learning tools to enable rapid development of materials and processes with little efforts. A robust high throughput in situ characterization guided ICME approach will help in accelerating process development for existing materials and processes and may also pave way for the development of new materials in the future. It is therefore important that the millennial metallurgist is acquainted with not just the handling of sophisticated characterization tools and multiscale simulation techniques but the ability to incorporate this expertise in the ML-AI paradigm to be relevant in the coming century.

8 Conclusions and Perspective

In situ experiments have provided better insights into the operative micro-mechanisms of different processes like solidification, deformation, recrystallization, solid-state phase transformation and failure in conventional metallic materials and helped in the development of new metallic materials like complex concentrated alloys and processes like different additive manufacturing processes. In situ characterization has played an important role in developing mechanistic mechanism-based crystal plasticity models or deformation and failure of metallic materials while data obtained from in situ experiments have helped tune models for solidification, recrystallization, phase transformation of metallic materials. Of particular interest are in situ characterization techniques offering hyperdimensional data from the real, reciprocal and compositional space that provides up-to-date information on different attributes of microstructure as a function of an external stimulus. Despite the tremendous advancement, there is a scope to add more peripherals to include different modes of loading and expand the range of process parameters like operating temperature, strain rate, strain path changes and cyclic loading as well as different environments to obtain information over a wide range of working conditions. There is a need to develop more such platforms and better the resolution as well as the data acquisition speed to capture real-time data. The huge data obtained from

in situ experiments coupled with microstructural simulations can be used to build machine learning models to cut down on further experiments thus paving way for the development of new processes for existing alloys as well as for the development of new metallic materials. Cradle to grave journey of a material observed using different in situ experiments in a short period of time can provide a mechanism map for different processes, accelerating development which can justify the high initial investment in operando techniques. In catalyst development there is a rational catalysis design wherein a new catalyst is developed from computations on the properties of the existing catalysts and a similar process is followed in the pharmaceutical industry¹²⁶. We believe the rational process and alloy development are possible within the ICME framework wherein high throughput in situ characterization experiments will play an important role and will become the bedrock for the sustainable development of metallic materials and processes in the future.

Publisher's Note

Springer Nature remains neutral with regard to jurisdictional claims in published maps and institutional affiliations.

Acknowledgements

The authors would like to acknowledge the generous funding from Science and Engineering Research Board, Department of Science and Technology, Government of India, Indian Space Research Organization for research on complex concentrated alloys. Thanks are due to the Society for Promotion of Academic and Research Collaborations, Ministry of Human Resource Development (SPARC, MHRD) for funding research on additive manufacturing while Tata Consultancy Services Research is acknowledged for funding high throughput experimentation research. Authors would like to thank facilities at the Advanced Centre for Materials Science and Advanced Imaging Centre at IIT Kanpur for providing in situ characterization experiments. K B would like to thank INSA-DFG for a fellowship to carry out some of the research presented here.

Declarations

Funding

Funding were provided by Science and Engineering Research Board (Grant Number: EMR/2016/006217, EMR/2016/006217, CRG/2020/003710),

Indian Space Research Organisation (Grant Number: STC/MET/2018047, STC/MET/2018041), Ministry of Human Resource Development (Grant Number: P1004 SPARC), and Tata Consultancy Services (Grant Number: TCS/MET/2017148).

Conflict of interest

The authors declare that they have no known competing financial interests or personal relationships that could have appeared to influence the work reported in this paper.

References

1. Ashby MF, Bréchet YJM, Cebon D, Salvo L (2004) Selection strategies for materials and processes. *Mater Des* 25:51–67. [https://doi.org/10.1016/S0261-3069\(03\)00159-6](https://doi.org/10.1016/S0261-3069(03)00159-6)
2. Ashby MF (2015) Materials and sustainable development. *Prog Nat Sci Mater Int*. [https://doi.org/10.1016/s1002-0071\(12\)60002-1](https://doi.org/10.1016/s1002-0071(12)60002-1)
3. Cann JL, De Luca A, Dunand DC, Dye D, Miracle DB, Oh HS, Olivetti EA, Pollock TM, Poole WJ, Yang R, Tasan CC (2021) Sustainability through alloy design: challenges and opportunities. *Prog Mater Sci* 117:100722. <https://doi.org/10.1016/j.pmatsci.2020.100722>
4. Raabe D, Tasan CC, Olivetti EA (2019) Strategies for improving the sustainability of structural metals. *Nature* 575:64–74. <https://doi.org/10.1038/s41586-019-1702-5>
5. Prior T, Giurco D, Mudd G, Mason L, Behrisch J (2012) Resource depletion, peak minerals and the implications for sustainable resource management. *Glob Environ Change* 22:577–587. <https://doi.org/10.1016/j.gloenvcha.2011.08.009>
6. Yellishetty M, Mudd GM (2014) Substance flow analysis of steel and long term sustainability of iron ore resources in Australia, Brazil, China and India. *J Clean Prod* 84:400–410. <https://doi.org/10.1016/j.jclepro.2014.02.046>
7. Ramakrishna S, Zhang TY, Lu WC, Qian Q, Low JSC, Yune JHR, Tan DZL, Bressan S, Sanvito S, Kalidindi SR (2019) Materials informatics. *J Intell Manuf* 30:2307–2326. <https://doi.org/10.1007/s10845-018-1392-0>
8. Dalenogare LS, Benitez GB, Ayala NF, Frank AG (2018) The expected contribution of Industry 4.0 technologies for industrial performance. *Int J Prod Econ* 204:383–394. <https://doi.org/10.1016/j.ijpe.2018.08.019>
9. Lasi H, Fettke P, Kemper HG, Feld T, Hoffmann M (2014) Industry 4.0. *Bus Inf Syst Eng* 6:239–242. <https://doi.org/10.1007/s12599-014-0334-4>
10. Ashima R, Haleem A, Bahl S, Javaid M, Mahla SK, Singh S (2021) Automation and manufacturing of smart materials in additive manufacturing technologies using internet of things towards the adoption of industry 4.0. *Mater Today Proc* 45:5081–5088. <https://doi.org/10.1016/j.matpr.2021.01.583>
11. Huang SH, Liu P, Mokasdar A, Hou L (2013) Additive manufacturing and its societal impact: a literature review. *Int J Adv Manuf Technol* 67:1191–1203. <https://doi.org/10.1007/s00170-012-4558-5>
12. Frazier WE (2014) Metal additive manufacturing: a review. *J Mater Eng Perform* 23:1917–1928. <https://doi.org/10.1007/s11665-014-0958-z>
13. Uriondo A, Esperon-Miguez M, Perinpanayagam S (2015) The present and future of additive manufacturing in the aerospace sector: a review of important aspects. *Proc Inst Mech Eng Part G J Aerosp Eng* 229:2132–2147. <https://doi.org/10.1177/0954410014568797>
14. Yi Wang W, Li J, Liu W, Liu ZK (2019) Integrated computational materials engineering for advanced materials: a brief review. *Comput Mater Sci* 158:42–48. <https://doi.org/10.1016/j.commatsci.2018.11.001>
15. de Pablo JJ, Jackson NE, Webb MA, Chen LQ, Moore JE, Morgan D, Jacobs R, Pollock T, Schlom DG, Toberer ES, Analytis J, Dabo I, DeLongchamp DM, Fiete GA, Grason GM, Hautier G, Mo Y, Rajan K, Reed EJ, Rodriguez E, Stevanovic V, Suntivich J, Thornton K, Zhao JC (2019) New frontiers for the materials genome initiative. *Comput Mater* 5:1–23. <https://doi.org/10.1038/s41524-019-0173-4>
16. Jain A, Persson KA, Ceder G (2016) Research update: the materials genome initiative: data sharing and the impact of collaborative ab initio databases. *APL Mater*. <https://doi.org/10.1063/1.4944683>
17. Liu Y, Niu C, Wang Z, Gan Y, Zhu Y, Sun S, Shen T (2020) Machine learning in materials genome initiative: a review. *J Mater Sci Technol* 57:113–122. <https://doi.org/10.1016/j.jmst.2020.01.067>
18. Nikolov S, Petrov M, Lymperakis L, Friák M, Sachs C, Fabritius HO, Raabe D, Neugebauer J (2010) Revealing the design principles of high-performance biological composites using Ab initio and multiscale simulations: the example of lobster cuticle. *Adv Mater* 22:519–526. <https://doi.org/10.1002/adma.200902019>
19. Roters F, Eisenlohr P, Hantcherli L, Tjahjanto DD, Bieler TR, Raabe D (2010) Overview of constitutive laws, kinematics, homogenization and multiscale methods in crystal plasticity finite-element modeling: theory, experiments, applications. *Acta Mater* 58:1152–1211. <https://doi.org/10.1016/j.actamat.2009.10.058>
20. Roters F, Eisenlohr P, Bieler TR, Raabe D. Crystal plasticity finite element methods (n.d.)
21. Raturi A, Aditya J, Gurao NP, Biswas K (2019) ICME approach to explore equiatomic and non-equiatomic single phase BCC refractory high entropy alloys. *J*

- Alloys Compd 806:587–595. <https://doi.org/10.1016/j.jallcom.2019.06.387>
22. Mohanty S, Samal S, Tazuddin A, Tiwary CS, Gurao NP, Biswas K (2015) Effect of processing route on phase stability in equiatomic multicomponent Ti₂₀Fe₂₀Ni₂₀Co₂₀Cu₂₀ high entropy alloy. *Mater Sci Technol (United Kingdom)* 31:1214–1222. <https://doi.org/10.1179/1743284715Y.0000000024>
 23. Gurao NP, Biswas K (2017) In the quest of single phase multi-component multiprincipal high entropy alloys. *J Alloys Compd* 697:434–442. <https://doi.org/10.1016/j.jallcom.2016.11.383>
 24. Gurao NP, Biswas K (2016) Deciphering micro-mechanisms of plastic deformation in a novel single phase fcc-based MnFeCoNiCu high entropy alloy using crystallographic texture. *Mater Sci Eng A* 657:224–233. <https://doi.org/10.1016/j.msea.2016.01.055>
 25. Raturi A, Biswas K, Gurao NP (2021) A mechanistic perspective on the kinetics of plastic deformation in FCC high entropy alloys: effect of strain, strain rate and temperature. *Scr Mater* 197:113809. <https://doi.org/10.1016/j.scriptamat.2021.113809>
 26. Akhil B, Bajpai A, Gurao NP, Biswas K (2021) Designing hexagonal close packed high entropy alloys using machine learning. *Model Simul Mater Sci Eng* 29:085005. <https://doi.org/10.1088/1361-651x/ac2b37>
 27. Hwang RC, Chen YJ, Huang HC (2010) Artificial intelligent analyzer for mechanical properties of rolled steel bar by using neural networks. *Expert Syst Appl* 37:3136–3139. <https://doi.org/10.1016/j.eswa.2009.09.069>
 28. Shen C, Wang C, Wei X, Li Y, van der Zwaag S, Xu W (2019) Physical metallurgy-guided machine learning and artificial intelligent design of ultrahigh-strength stainless steel. *Acta Mater* 179:201–214. <https://doi.org/10.1016/j.actamat.2019.08.033>
 29. Zou C, Li J, Wang WY, Zhang Y, Lin D, Yuan R, Wang X, Tang B, Wang J, Gao X, Kou H, Hui X, Zeng X, Qian M, Song H, Liu ZK, Xu D (2021) Integrating data mining and machine learning to discover high-strength ductile titanium alloys. *Acta Mater* 202:211–221. <https://doi.org/10.1016/j.actamat.2020.10.056>
 30. Zhou Z, Zhou Y, He Q, Ding Z, Li F, Yang Y (2019) Machine learning guided appraisal and exploration of phase design for high entropy alloys. *Npj Comput Mater* 5:1–9. <https://doi.org/10.1038/s41524-019-0265-1>
 31. Xu W, Brandt M, Sun S, Elambasseril J, Liu Q, Latham K, Xia K, Qian M (2015) Additive manufacturing of strong and ductile Ti-6Al-4V by selective laser melting via in situ martensite decomposition. *Acta Mater* 85:74–84. <https://doi.org/10.1016/j.actamat.2014.11.028>
 32. Sinha S, Gurao NP (2017) In situ electron backscatter diffraction study of twinning in commercially pure titanium during tension-compression deformation and annealing. *Mater Des* 116:686–693. <https://doi.org/10.1016/j.matdes.2016.10.060>
 33. Attar H, Bönisch M, Calin M, Zhang LC, Scudino S, Eckert J (2014) Selective laser melting of in situ titanium-titanium boride composites: processing, microstructure and mechanical properties. *Acta Mater* 76:13–22. <https://doi.org/10.1016/j.actamat.2014.05.022>
 34. Zakhosheva M, Schmitt LA, Acosta M, Guo H, Jo W, Schierholz R, Kleebe HJ, Tan X (2015) Wide compositional range in situ electric field investigations on lead-free Ba (Zr_{0.2}Ti_{0.8})O_{3-x}(Ba_{0.7}Ca_{0.3})TiO₃ piezoceramic wide compositional range in situ. *Phys Rev Appl* 3:1–12. <https://doi.org/10.1103/PhysRevApplied.3.064018>
 35. Reddy MV, Paul JP, Sowmya NS, Srinivas A, Das D (2016) Magneto-electric properties of in-situ prepared xCoFe₂O₄-(1-x)(Ba_{0.85}Ca_{0.15})(Zr_{0.1}Ti_{0.9})O₃ particulate composites. *Ceram Int* 42:17827–17833. <https://doi.org/10.1016/j.ceramint.2016.08.112>
 36. Nagase T, Rack PD, Noh JH, Egami T (2015) In-situ TEM observation of structural changes in nano-crystalline CoCrCuFeNi multicomponent high-entropy alloy (HEA) under fast electron irradiation by high voltage electron microscopy (HVEM). *Intermetallics* 59:32–42. <https://doi.org/10.1016/j.intermet.2014.12.007>
 37. Nagarajan S, Jain R, Gurao NP (2021) Microstructural characteristics governing the lattice rotation in Al-Mg alloy using in-situ EBSD. *Mater Charact* 180:111405. <https://doi.org/10.1016/j.matchar.2021.111405>
 38. Raturi A, Biswas K, Gurao NP (2022) Elastic and plastic anisotropy in a refractory high entropy alloy utilizing combinatorial instrumented indentation and electron backscatter diffraction. *J Alloys Compd* 896:162902. <https://doi.org/10.1016/j.jallcom.2021.162902>
 39. Chakrabarty A, Kumar V, Anindya S, Shreya D, Nilesh M, Gurao P (2021) Study of the effect of two separate tilt angles of laser scanning lines on the microstructure and mechanical properties in direct metal laser sintered AlSi10Mg alloy. *Met Mater Int*. <https://doi.org/10.1007/s12540-021-01080-w>
 40. Ghosh A, Sahu VK, Gurao NP (2021) Effect of heat treatment on the ratcheting behaviour of additively manufactured and thermo-mechanically treated Ti-6Al-4V alloy. *Mater Sci Eng A*. <https://doi.org/10.1016/j.msea.2021.142345>
 41. Bahadur F, Jain R, Biswas K, Gurao NP (2022) Low cycle fatigue behaviour of non-equiatomic TRIP dual-phase Fe₅₀Mn₃₀Co₁₀Cr₁₀ high entropy alloy. *Int J Fatigue* 155:106545. <https://doi.org/10.1016/j.ijfatigue.2021.106545>
 42. Gurao NP, Akhiani H, Szpunar JA (2014) Pilgering of Zircaloy-4: experiments and simulations. *J Nucl Mater* 453:158–168. <https://doi.org/10.1016/j.jnucmat.2014.06.047>
 43. Sahu VK, Gupta S, Gurao NP (2020) Effect of initial texture on the evolution of microstructure and

- texture during rolling of commercially pure titanium at room and cryogenic temperature. *Metall Mater Trans A*. <https://doi.org/10.1007/s11661-020-05979-8>
44. Sinha S, Sahu VK, Beura V, Sonkusare R, Kalsar R, Das AKL, Basu J, Gurao NP, Biswas K (2021) Initial texture dependence of nanocrystalline omega phase formation during high pressure torsion of commercially pure titanium. *Mater Sci Eng A* 802:140687. <https://doi.org/10.1016/j.msea.2020.140687>
 45. Sonkusare R, Divya Janani P, Gurao NP, Sarkar S, Sen S, Pradeep KG, Biswas K (2018) Phase equilibria in equiatomic CoCuFeMnNi high entropy alloy. *Mater Chem Phys* 210:269–278. <https://doi.org/10.1016/j.matchemphys.2017.08.051>
 46. Sonkusare R, Swain A, Rahul MR, Samal S, Gurao NP, Biswas K, Singh SS, Nayan N (2019) Establishing processing-microstructure-property paradigm in complex concentrated equiatomic CoCuFeMnNi alloy. *Mater Sci Eng A* 759:415–429. <https://doi.org/10.1016/j.msea.2019.04.096>
 47. Booth MJ (2014) Adaptive optical microscopy: the ongoing quest for a perfect image. *Light Sci Appl* 3:1–7. <https://doi.org/10.1038/lsa.2014.46>
 48. Goodhew PJ, Humphreys J, Beanland R (2001) Electron microscopy and analysis
 49. Williams DB, Carter CB (2009) Transmission electron microscopy: a textbook for materials science. https://doi.org/10.1007/978-1-4757-2519-3_6
 50. Goldstein JI, Newbury DE, Michael JR, Ritchie NWM, Scott JHJ, Joy DC (2003) Scanning electron microscopy and x-ray microanalysis. <https://doi.org/10.1007/978-1-4939-6676-9>
 51. Patterson BM, Cordes NL, Henderson K, Mertens JCE, Clarke AJ, Hornberger B, Merkle A, Etchin S, Tkachuk A, Leibowitz M, Trapp D, Qiu W, Zhang B, Bale H, Lu X, Hartwell R, Withers PJ, Bradley RS (2016) In situ laboratory-based transmission X-ray microscopy and tomography of material deformation at the nanoscale. *Exp Mech* 56:1585–1597. <https://doi.org/10.1007/s11340-016-0197-3>
 52. Holt M, Harder R, Winarski R, Rose V (2013) Nanoscale hard X-ray microscopy methods for materials studies*. *Annu Rev Mater Res* 43:183–211. <https://doi.org/10.1146/annurev-matsci-071312-121654>
 53. Grunwaldt JD, Schroer CG (2010) Hard and soft X-ray microscopy and tomography in catalysis: Bridging the different time and length scales. *Chem Soc Rev* 39:4741–4753. <https://doi.org/10.1039/c0cs00036a>
 54. Nervo L, King A, Fitzner A, Ludwig W, Preuss M (2016) A study of deformation twinning in a titanium alloy by X-ray diffraction contrast tomography. *Acta Mater* 105:417–428. <https://doi.org/10.1016/j.actamat.2015.12.032>
 55. Bilderback DH, Elleaume P, Weckert E (2005) Review of third and next generation synchrotron light sources. *J Phys B At Mol Opt Phys*. <https://doi.org/10.1088/0953-4075/38/9/022>
 56. Engler O, Randle V (2010) Introduction to texture analysis. https://doi.org/10.1142/9781848161160_0001
 57. Suwas S, Ray RK, Satyam Suwas RKR (2014) Crystallographic texture of materials. <https://books.google.be/books?id=peRKBAAAQBAJ&dq=Crystallographic+Texture+of+Materials&hl=en&sa=X&ei=FqzGVLySH8zdPevEgBA&ved=0CCAQ6AEwAA>
 58. Chen B, Zhang H, Xuan J, Offer GJ, Wang H (2020) Seeing is believing: in situ/operando optical microscopy for probing electrochemical energy systems. *Adv Mater Technol* 5:1–21. <https://doi.org/10.1002/admt.20200555>
 59. Sinha S, Szpunar JA, Kiran Kumar NAP, Gurao NP (2015) Tensile deformation of 316L austenitic stainless steel using in-situ electron backscatter diffraction and crystal plasticity simulations. *Mater Sci Eng A* 637:48–55. <https://doi.org/10.1016/j.msea.2015.04.005>
 60. Ubhi HS, Parsons J, Othen N, Campbell S, Poole R, Gholinia A (2014) In-situ EBSD phase transformation and recrystallisation. *J Phys Conf Ser* 522:8–11. <https://doi.org/10.1088/1742-6596/522/1/012011>
 61. Kalácska S, Dankházi Z, Zilahi G, Maeder X, Michler J, Ispánovity PD, Groma I (2020) Investigation of geometrically necessary dislocation structures in compressed Cu micropillars by 3-dimensional HR-EBSD. *Mater Sci Eng A*. <https://doi.org/10.1016/j.msea.2019.138499>
 62. Ray RK, Hutchinson WB, Duggan BJ (1975) A study of the nucleation of recrystallization using HVEM. *Acta Metall* 23:831–840. [https://doi.org/10.1016/0001-6160\(75\)90199-6](https://doi.org/10.1016/0001-6160(75)90199-6)
 63. Tiwari K, Biswas K, Palliwal M, Majumdar B (2020) Melting behaviour of tri-phasic Bi 44 In 32 Sn 23 alloy nanoparticle embedded in icosahedral quasicrystalline matrix. *J Alloys Compd* 834:155160. <https://doi.org/10.1016/j.jallcom.2020.155160>
 64. Shan ZW, Mishra RK, Syed Asif SA, Warren OL, Minor AM (2008) Mechanical annealing and source-limited deformation in submicrometre-diameter Nicrystals. *Nat Mater* 7:115–119. <https://doi.org/10.1038/nmat2085>
 65. Cullity BD (1956) Elements of X-ray diffraction, vol 8. Addison-Wesley, Reading, pp 237–238. <https://doi.org/10.1088/0031-9112/8/7/008>
 66. Murphy-Leonard AD, Pagan DC, Callahan PG, Heinkel ZK, Jasien CE, Rowenhorst DJ (2021) Investigation of porosity, texture, and deformation behavior using high energy X-rays during in-situ tensile loading in additively manufactured 316L stainless steel. *Mater Sci Eng A* 810:141034. <https://doi.org/10.1016/j.msea.2021.141034>
 67. Cornelius TW, Thomas O (2018) Progress of in situ synchrotron X-ray diffraction studies on the mechanical behavior of materials at small scales. *Prog Mater*

- Sci 94:384–434. <https://doi.org/10.1016/j.pmatsci.2018.01.004>
68. Zhang H, Jérusalem A, Salvati E, Papadaki C, Fong KS, Song X, Korsunsky AM (2019) Multi-scale mechanisms of twinning-detwinning in magnesium alloy AZ31B simulated by crystal plasticity modeling and validated via in situ synchrotron XRD and in situ SEM-EBSD. *Int J Plast* 119:43–56. <https://doi.org/10.1016/j.ijplas.2019.02.018>
 69. Krishna MV, Sahu VK, Ghosh A, Brokmeier HG, Gurao NP (2020) In-situ investigation of the evolution of microstructure and texture during load reversal of commercially pure titanium using synchrotron X-ray diffraction. *Mater Charact* 159:110039. <https://doi.org/10.1016/j.matchar.2019.110039>
 70. Hsu WN, Polatidis E, Šmíd M, Casati N, Van Petegem S, Van Swygenhoven H (2018) Load path change on superelastic NiTi alloys: in situ synchrotron XRD and SEM DIC. *Acta Mater* 144:874–883. <https://doi.org/10.1016/j.actamat.2017.11.035>
 71. Ma L, Wang L, Nie Z, Wang F, Xue Y, Zhou J, Cao T, Wang Y, Ren Y (2017) Reversible deformation-induced martensitic transformation in Al_{0.6}CoCrFeNi high-entropy alloy investigated by in situ synchrotron-based high-energy X-ray diffraction. *Acta Mater* 128:12–21. <https://doi.org/10.1016/j.actamat.2017.02.014>
 72. Kenel C, Grolimund D, Fife JL, Samson VA, Van Petegem S, Van Swygenhoven H, Leinenbach C (2016) Combined in situ synchrotron micro X-ray diffraction and high-speed imaging on rapidly heated and solidified Ti-48Al under additive manufacturing conditions. *Scr Mater* 114:117–120. <https://doi.org/10.1016/j.scriptamat.2015.12.009>
 73. Sonkusare R, Biswas K, Al-Hamdany N, Brokmeier HG, Kalsar R, Schell N, Gurao NP (2020) A critical evaluation of microstructure-texture-mechanical behavior heterogeneity in high pressure torsion processed CoCuFeMnNi high entropy alloy. *Mater Sci Eng A* 782:139187. <https://doi.org/10.1016/j.msea.2020.139187>
 74. Zhang XX, Ni DR, Xiao BL, Andrä H, Gan WM, Hofmann M, Ma ZY (2015) Determination of macroscopic and microscopic residual stresses in friction stir welded metal matrix composites via neutron diffraction. *Acta Mater* 87:161–173. <https://doi.org/10.1016/j.actamat.2015.01.006>
 75. Woo W, An GB, Kingston EJ, Dewald AT, Smith DJ, Hill MR (2013) Through-thickness distributions of residual stresses in two extreme heat-input thick welds: a neutron diffraction, contour method and deep hole drilling study. *Acta Mater* 61:3564–3574. <https://doi.org/10.1016/j.actamat.2013.02.034>
 76. Wang Z, Chen J, Besnard C, Kunčická L, Kocich R, Korsunsky AM (2021) In situ neutron diffraction investigation of texture-dependent shape memory effect in a near equiatomic NiTi alloy. *Acta Mater* 202:135–148. <https://doi.org/10.1016/j.actamat.2020.10.049>
 77. Wain N, Radaelli PG, Todd RI (2007) In situ neutron diffraction study of residual stress development in MgO/SiC ceramic nanocomposites during thermal cycling. *Acta Mater* 55:4535–4544. <https://doi.org/10.1016/j.actamat.2007.04.018>
 78. Le Hong T, Turque I, Brachet JC, Crépin J, André G, Barres Q, Guillou R, Toffolon-Masclat C, Joubert JM, Le Saux M (2020) Phase transformations during cooling from the β Zr phase temperature domain in several hydrogen-enriched zirconium alloys studied by in situ and ex situ neutron diffraction. *Acta Mater* 199:453–468. <https://doi.org/10.1016/j.actamat.2020.08.061>
 79. Michalak B, Sommer H, Mannes D, Kaestner A, Brezesinski T, Janek J (2015) Gas evolution in operating lithium-ion batteries studied in situ by neutron imaging. *Sci Rep* 5:1–9. <https://doi.org/10.1038/srep15627>
 80. Aggarwal A, Chouhan A, Patel S, Yadav DK, Kumar A, Vinod AR, Prashanth KG, Gurao NP (2020) Role of impinging powder particles on melt pool hydrodynamics, thermal behaviour and microstructure in laser-assisted DED process: a particle-scale DEM–CFD–CA approach. *Int J Heat Mass Transf* 158:119989. <https://doi.org/10.1016/j.ijheatmasstransfer.2020.119989>
 81. Chakrabarty A, Chakraborty P, Sahu VK, Gurao NP, Khutia N (2021) Investigation of strain localization in additively manufactured AlSi10Mg using CPFEM. In: *Compos. Mater. Extrem. Load.*, Springer, Singapore, pp 199–214. https://doi.org/10.1007/978-981-16-4138-1_15
 82. Miracle DB, Miller JD, Senkov ON, Woodward C, Uchic MD, Tiley J (2014) Exploration and development of high entropy alloys for structural applications. *Entropy* 16:494–525. <https://doi.org/10.3390/e16010494>
 83. Miracle DB, Senkov ON (2017) A critical review of high entropy alloys and related concepts. *Acta Mater* 122:448–511. <https://doi.org/10.1016/j.actamat.2016.08.081>
 84. Cantor B, Chang ITH, Knight P, Vincent AJB (2004) Microstructural development in equiatomic multi-component alloys. *Mater Sci Eng A* 375–377:213–218. <https://doi.org/10.1016/j.msea.2003.10.257>
 85. Yeh JW, Chen SK, Lin SJ, Gan JY, Chin TS, Shun TT, Tsau CH, Chang SY (2004) Nanostructured high-entropy alloys with multiple principal elements: Novel alloy design concepts and outcomes. *Adv Eng Mater* 6:299–303. <https://doi.org/10.1002/adem.200300567>
 86. Tsai MH, Yeh JW (2014) High-entropy alloys: a critical review. *Mater Res Lett* 2(3):107–123
 87. Agarwal R, Sonkusare R, Jha SR, Gurao NP, Biswas K, Nayan N (2018) Understanding the deformation behavior of CoCuFeMnNi high entropy alloy by investigating mechanical properties of binary ternary and quaternary alloy subsets. *Mater Des* 157:539–550. <https://doi.org/10.1016/j.matdes.2018.07.046>

88. Mohanty S, Gurao NP, Padaikathan P, Biswas K (2017) Ageing behaviour of equiatomic consolidated Al₂₀Co-20Cu₂₀Ni₂₀Zn₂₀ high entropy alloy. *Mater Charact* 129:127–134. <https://doi.org/10.1016/j.matchar.2017.04.011>
89. Ghassemali E, Sonkusare R, Biswas K, Gurao NP (2018) Dynamic precipitation at elevated temperatures in a dual-phase AlCoCrFeNi high-entropy alloy: an in situ study. *Philos Mag Lett* 98:400–409. <https://doi.org/10.1080/09500839.2018.1563728>
90. Mohanty S, Maity TN, Mukhopadhyay S, Sarkar S, Gurao NP, Bhowmick S, Biswas K (2017) Powder metallurgical processing of equiatomic AlCoCrFeNi high entropy alloy: microstructure and mechanical properties. *Mater Sci Eng A* 679:299–313. <https://doi.org/10.1016/j.msea.2016.09.062>
91. Jha SR, Biswas K, Gurao NP (2021) Achieving high strength and ductility in equimolar FeMnNi medium entropy alloy by tuning microstructural entropy. *Mater Sci Eng A* 826:141965. <https://doi.org/10.1016/j.msea.2021.141965>
92. Sonkusare R, Jain R, Biswas K, Parameswaran V, Gurao NP (2020) High strain rate compression behaviour of single phase CoCuFeMnNi high entropy alloy. *J Alloys Compd* 823:153763. <https://doi.org/10.1016/j.jallcom.2020.153763>
93. Bahadur F, Biswas K, Gurao NP (2020) Micro-mechanisms of microstructural damage due to low cycle fatigue in CoCuFeMnNi high entropy alloy. *Int J Fatigue* 130:105258. <https://doi.org/10.1016/j.ijfatigue.2019.105258>
94. Ghassemali E, Sonkusare R, Biswas K, Gurao NP (2017) In-situ study of crack initiation and propagation in a dual phase AlCoCrFeNi high entropy alloy. *J Alloys Compd* 710:539–546. <https://doi.org/10.1016/j.jallcom.2017.03.307>
95. Yang F, Dong L, Hu X, Zhou XF, Fang F, Xie Z, Jiang J (2020) Microstructural features and tensile behaviors of a novel FeMnCoCr high entropy alloys. *Mater Lett* 275:128154. <https://doi.org/10.1016/j.matlet.2020.128154>
96. Xu N, Li S, Li R, Zhang M, Yan Z, Cao Y, Nie Z, Ren Y, Wang YD (2020) In situ investigation of the deformation behaviors of Fe₂₀Co₃₀Cr₂₅Ni₂₅ and Fe₂₀Co₃₀Cr₃₀Ni₂₀ high entropy alloys by high-energy X-ray diffraction. *Mater Sci Eng A* 795:139936. <https://doi.org/10.1016/j.msea.2020.139936>
97. Wang Y, Liu B, Yan K, Wang M, Kabra S, Chiu YL, Dye D, Lee PD, Liu Y, Cai B (2018) Probing deformation mechanisms of a FeCoCrNi high-entropy alloy at 293 and 77 K using in situ neutron diffraction. *Acta Mater* 154:79–89. <https://doi.org/10.1016/j.actamat.2018.05.013>
98. Cai B, Liu B, Kabra S, Wang Y, Yan K, Lee PD, Liu Y (2017) Deformation mechanisms of Mo alloyed FeCoCrNi high entropy alloy: In situ neutron diffraction. *Acta Mater* 127:471–480. <https://doi.org/10.1016/j.actamat.2017.01.034>
99. Wu Y, Liu WH, Wang XL, Ma D, Stoica AD, Nieh TG, He ZB, Lu ZP (2014) In-situ neutron diffraction study of deformation behavior of a multi-component high-entropy alloy. *Appl Phys Lett*. <https://doi.org/10.1063/1.4863748>
100. Fu S, Bei H, Chen Y, Liu TK, Yu D, An K (2018) Deformation mechanisms and work-hardening behavior of transformation-induced plasticity high entropy alloys by in-situ neutron diffraction. *Mater Res Lett* 6:620–626. <https://doi.org/10.1080/21663831.2018.1523239>
101. Naeem M, He H, Zhang F, Huang H, Harjo S, Kawasaki T, Wang B, Lan S, Wu Z, Wang F, Wu Y, Lu Z, Zhang Z, Liu CT, Wang XL (2020) Cooperative deformation in high-entropy alloys at ultralow temperatures. *Sci Adv*. <https://doi.org/10.1126/sciadv.aax4002>
102. Vaezi M, Seitz H, Yang S (2013) A review on 3D micro-additive manufacturing technologies. *Int J Adv Manuf Technol* 67:1721–1754. <https://doi.org/10.1007/s00170-012-4605-2>
103. Li N, Huang S, Zhang G, Qin R, Liu W, Xiong H, Shi G, Blackburn J (2019) Progress in additive manufacturing on new materials: a review. *J Mater Sci Technol* 35:242–269. <https://doi.org/10.1016/j.jmst.2018.09.002>
104. Epp J, Dong J, Meyer H, Bohlen A (2020) Analysis of cyclic phase transformations during additive manufacturing of hardenable tool steel by in-situ X-ray diffraction experiments. *Scr Mater* 177:27–31. <https://doi.org/10.1016/j.scriptamat.2019.09.021>
105. Liu Y, Yang Y, Wang D (2016) A study on the residual stress during selective laser melting (SLM) of metallic powder. *Int J Adv Manuf Technol* 87:647–656. <https://doi.org/10.1007/s00170-016-8466-y>
106. Loh LE, Chua CK, Yeong WY, Song J, Mapar M, Sing SL, Liu ZH, Zhang DQ (2015) Numerical investigation and an effective modelling on the selective laser melting (SLM) process with aluminium alloy 6061. *Int J Heat Mass Transf* 80:288–300. <https://doi.org/10.1016/j.ijheatmasstransfer.2014.09.014>
107. Yang J, Yu H, Yin J, Gao M, Wang Z, Zeng X (2016) Formation and control of martensite in Ti-6Al-4V alloy produced by selective laser melting. *Mater Des* 108:308–318. <https://doi.org/10.1016/j.matdes.2016.06.117>
108. Kaschel FR, Vijayaraghavan RK, Shmeliov A, McCarrthy EK, Canavan M, McNally PJ, Dowling DP, Nicolosi V, Celikin M (2020) Mechanism of stress relaxation and phase transformation in additively manufactured Ti-6Al-4V via in situ high temperature XRD and TEM analyses. *Acta Mater* 188:720–732. <https://doi.org/10.1016/j.actamat.2020.02.056>
109. Ungár T (2004) Microstructural parameters from X-ray diffraction peak broadening. *Scr Mater* 51:777–781. <https://doi.org/10.1016/j.scriptamat.2004.05.007>

110. Ma T, Ge J, Chen Y, Jin T, Lei Y (2019) Observation of in-situ tensile wire-arc additively manufactured 205A aluminum part: 3D pore characteristics and microstructural evolution. *Mater Lett* 237:266–269. <https://doi.org/10.1016/j.matlet.2018.11.115>
111. Kong D, Dong C, Ni X, Liang Z, Li X (2021) In-situ observation of asymmetrical deformation around inclusion in a heterogeneous additively manufactured 316L stainless steel. *J Mater Sci Technol* 89:133–140. <https://doi.org/10.1016/j.jmst.2021.02.022>
112. Murr LE, Gaytan SM, Ramirez DA, Martinez E, Hernandez J, Amato KN, Shindo PW, Medina FR, Wicker RB (2012) Metal fabrication by additive manufacturing using laser and electron beam melting technologies. *J Mater Sci Technol* 28:1–14. [https://doi.org/10.1016/S1005-0302\(12\)60016-4](https://doi.org/10.1016/S1005-0302(12)60016-4)
113. Slotwinski JA, Garboczi EJ, Stutzman PE, Ferraris CF, Watson SS, Peltz MA (2014) Characterization of metal powders used for additive manufacturing. *J Res Natl Inst Stand Technol* 119:460–493. <https://doi.org/10.6028/jres.119.018>
114. Wang Y, Liang K, van de Water W, Marques W, Ubachs W (2018) Rayleigh–Brillouin light scattering spectroscopy of nitrous oxide (N₂O). *J Quant Spectrosc Radiat Transf* 206:63–69. <https://doi.org/10.1016/j.jqsrt.2017.10.029>
115. Sun Y, Hebert RJ, Aindow M (2018) Non-metallic inclusions in 17–4PH stainless steel parts produced by selective laser melting. *Mater Des* 140:153–162. <https://doi.org/10.1016/j.matdes.2017.11.063>
116. Kong D, Dong C, Ni X, Zhang L, Yao J, Man C, Cheng X, Xiao K, Li X (2019) Mechanical properties and corrosion behavior of selective laser melted 316L stainless steel after different heat treatment processes. *J Mater Sci Technol* 35:1499–1507. <https://doi.org/10.1016/j.jmst.2019.03.003>
117. Kong D, Ni X, Dong C, Zhang L, Man C, Yao J, Xiao K, Li X (2018) Heat treatment effect on the microstructure and corrosion behavior of 316L stainless steel fabricated by selective laser melting for proton exchange membrane fuel cells. *Electrochim Acta* 276:293–303. <https://doi.org/10.1016/j.electacta.2018.04.188>
118. de Formanoir C, Michotte S, Rigo O, Germain L, Godet S (2016) Electron beam melted Ti-6Al-4V: microstructure, texture and mechanical behavior of the as-built and heat-treated material. *Mater Sci Eng A* 652:105–119. <https://doi.org/10.1016/j.msea.2015.11.052>
119. Kok Y, Tan XP, Wang P, Nai MLS, Loh NH, Liu E, Tor SB (2018) Anisotropy and heterogeneity of microstructure and mechanical properties in metal additive manufacturing: a critical review. *Mater Des* 139:565–586. <https://doi.org/10.1016/j.matdes.2017.11.021>
120. Antonysamy AA, Meyer J, Prangnell PB (2013) Effect of build geometry on the β -grain structure and texture in additive manufacture of Ti6Al4V by selective electron beam melting. *Mater Charact* 84:153–168. <https://doi.org/10.1016/j.matchar.2013.07.012>
121. Banerjee D, Williams JC (2013) Perspectives on titanium science and technology. *Acta Mater* 61:844–879. <https://doi.org/10.1016/j.actamat.2012.10.043>
122. Liu Z, Zhao Z, Liu J, Wang L, Yang G, Gong S, Wang Q, Yang R (2019) Effect of α texture on the tensile deformation behavior of Ti-6Al-4V alloy produced via electron beam rapid manufacturing. *Mater Sci Eng A* 742:508–516. <https://doi.org/10.1016/j.msea.2018.11.012>
123. Schwalbe KH (1977) On the influence of microstructure on crack propagation mechanisms and fracture toughness of metallic materials. *Eng Fract Mech* 9:795–832. [https://doi.org/10.1016/0013-7944\(77\)90004-2](https://doi.org/10.1016/0013-7944(77)90004-2)
124. Liu Z, Zhao ZB, Liu J, Wang Q, Guo Z, Zeng Y, Yang G, Gong S (2021) Effects of the crystallographic and spatial orientation of α lamellae on the anisotropic in-situ tensile behaviors of additive manufactured Ti-6Al-4V. *J Alloys Compd* 850:156886. <https://doi.org/10.1016/j.jallcom.2020.156886>
125. Santos LPM, Béréš M, Bastos IN, Tavares SSM, Abreu HFG, Gomes da Silva MJ (2015) Hydrogen embrittlement of ultra high strength 300 grade maraging steel. *Corros Sci* 101:12–18. <https://doi.org/10.1016/j.corsci.2015.06.022>
126. Li S, Liu M, Ren Y, Wang Y (2019) Hydrogen embrittlement behaviors of additive manufactured maraging steel investigated by in situ high-energy X-ray diffraction. *Mater Sci Eng A* 766:1–13. <https://doi.org/10.1016/j.msea.2019.138341>
127. Grajciar L, Heard CJ, Bondarenko AA, Polynski MV, Meeprasert J, Pidko EA, Nachtigall P (2018) Towards operando computational modeling in heterogeneous catalysis. *Chem Soc Rev* 47:8307–8348. <https://doi.org/10.1039/c8cs00398j>

